viability was measured with the use of a WST-8 kit (Nacalai Tesque, Kyoto, Japan).

3. Results

3.1. Infection of iPS-Hep cells with HCVpv

HCV entry requires sequential interaction between the envelope proteins and multiple cellular factors, including CD81, SR-BI, claudin-1, and occludin [29]. To investigate expression of these receptors in iPS-Hep cells, we performed RT-PCR analysis. iPS cells expressed CD81 and occludin, but not SR-BI and claudin-1. In contrast, iPS-Hep and Huh7 cells expressed all four receptors (Fig. 1A). HCVpv have been widely used in studies of the mechanism of HCV entry and in screens for inhibitors of HCV infection [30]. We therefore investigated HCVpv infection in iPS-Hep cells. iPS cells showed no susceptibility to HCVpv infection. In contrast, HCVpv dose-dependently infected iPS-Hep cells as well as Huh7 cells, a popular model cell line for HCV research (Fig. 1B). Treatment of the cells with IgG did not affect susceptibility of iPS-Hep or Huh7 cells to HCVpv infection, even at IgG concentrations of 1 μg/ml. In contrast, anti-CD81 antibody dose-dependently inhibited HCVpv infection of iPS-Hep and Huh7 cells, and the antibody treatment did not affect infection of VSVpv with iPS-Hep (Fig. 1C). These findings suggest that iPS-Hep cells are a useful model for HCV infection.

3.2. Replication of subgenomic HCV RNA in iPS-Hep cells

We previously developed Ad vectors containing tet-controllable and RNA pol I-driven HCV RNA subgenomic replicons (AdP$_i$235-HCV [replication competent], and AdP$_i$235-ΔGDD [replication incompetent]). The replicons encoded luciferase, and monitoring of luciferase activity in infected cells was a simple and convenient method to evaluate HCV replication [24]. Here, we found cells transduced with the replication-competent HCV replicon expressed luciferase in iPS-Hep cells, but not in iPS cells (Fig. 2A). In contrast, cells transduced with the replication-incompetent HCV replicon did not express luciferase (Fig. 2A). Taken together, these results suggest that replication of the HCV RNA genome occurred in the iPS-Hep cells. To confirm replication of the HCV genome, we investigated production of minus-strand HCV RNA from the positive-strand HCV RNA genome by performing real time-PCR analysis. The results of this analysis showed that minus-strand HCV RNA was produced in iPS-Hep cells and Huh7 cells, but not in iPS cells (Fig. 2B). To investigate whether the iPS-Hep cells could be used to screen for drugs that suppress HCV replication, we treated the cells with a suppressor of HCV replication, IFN. Treatment with IFN resulted in dose-dependent attenuated replication of the HCV genome with no cytotoxicity (Fig. 3A and B). These findings suggest that the iPS-Hep cells are a suitable system to use for monitoring the replication of the HCV RNA genome.

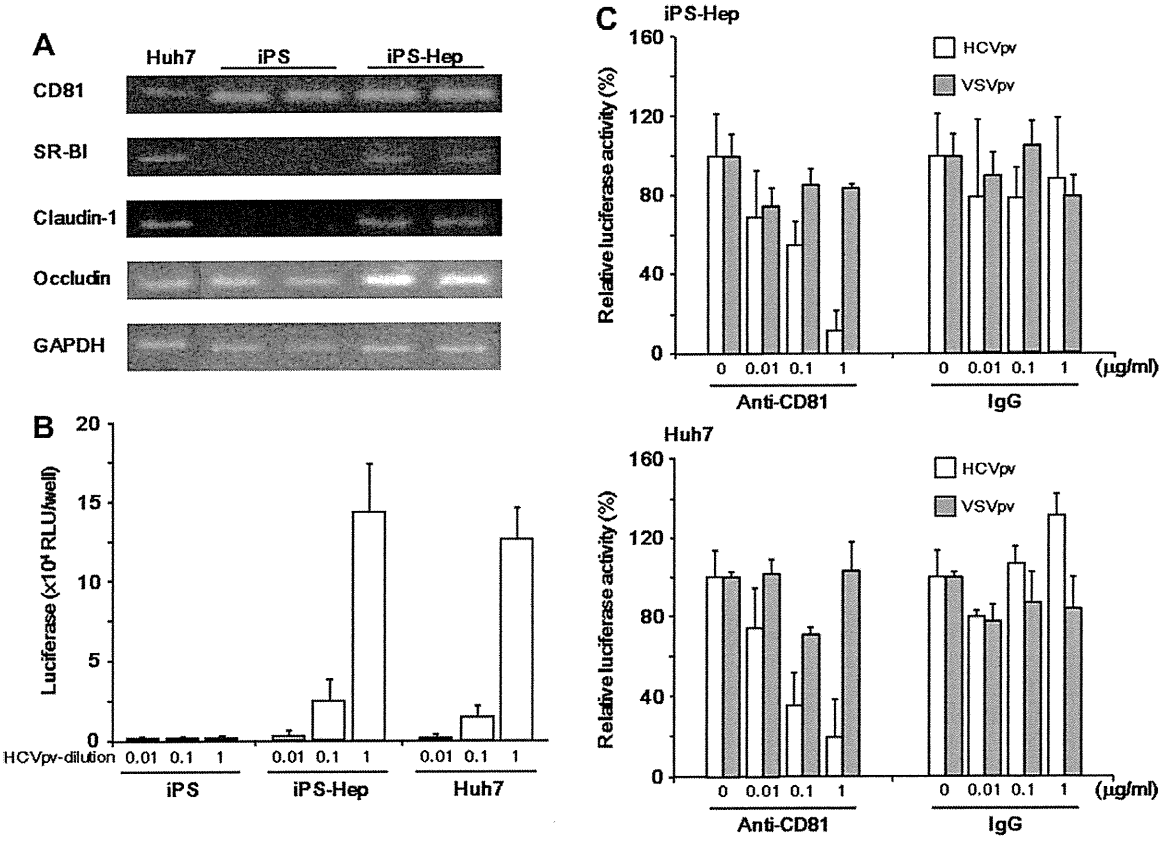

Fig. 1. HCV infection assay in iPS-Hep cells. (A) Expression of HCV receptors in iPS-Hep cells. Total RNA samples from Huh7, iPS, and iPS-Hep cells were subjected to RT-PCR analysis as described in the Section 2. The PCR products were separated on 2% agarose gels, followed by staining with ethidium bromide. (B) Infection of iPS-Hep cells with HCVpv. iPS, iPS-Hep and Huh7 cells were infected with HCVpv at the indicated dilution. After 2 h of infection, the cells were cultured with fresh medium for 24 h. Then, luciferase activities were measured. Data are presented as means ± SD (n = 3). (C) Effect of anti-CD81 antibody on infection of iPS-Hep cells with HCVpv. iPS-Hep (upper panel) and Huh7 (lower panel) cells were treated with mixtures of HCVpv (open column) or VSVpv (gray column) and anti-CD81 antibody or control mouse IgG at the indicated concentrations. After a 2-h incubation, the cells were cultured with fresh medium for 24 h. Then, the luciferase activities were measured. Data represent the percentage of vehicle-treated cells. Data are presented as means ± SD (n = 3).

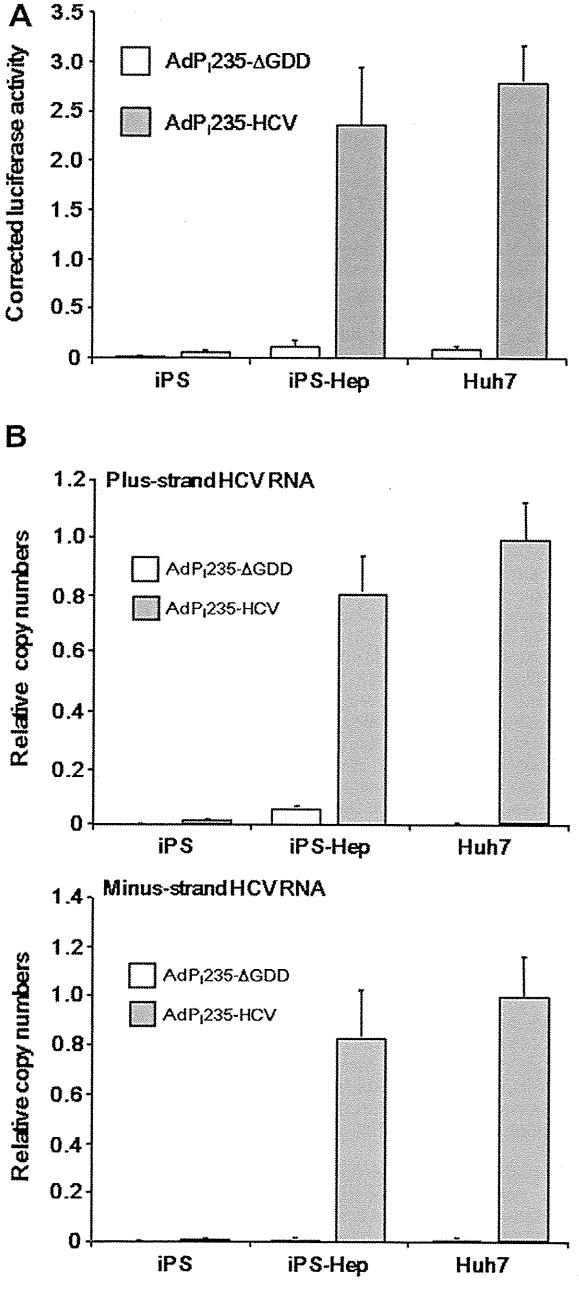

Fig. 2. HCV replication assay in iPS-Hep cells. (A) Comparison of replication of HCV subgenomic replicons, AdP$_i$235-HCV (gray column) and AdP$_i$235-ΔGDD (open column), in iPS, iPS-Hep and Huh7 cells. The cells were infected with replicons, treated with Dox, and renilla luciferase activity was measured, as described in the Section 2. To normalize for infectivity of Ad vector, cells were co-infected with AdP$_i$235-fluc and Ad-tTA. After 72 h, firefly luciferase activity was measured. Corrected luciferase activity was calculated as the ratio of renilla luciferase activity to firefly luciferase activity. (B) Real-time PCR analysis of HCV plus- and minus-strand RNA in iPS-Hep cells. iPS-Hep cells were infected with replicons, and total RNA was subjected to real-time PCR analysis, as described in the Section 2. The copy numbers were shown as ratio of those of Huh7. Data are presented as means ± SD (n = 3).

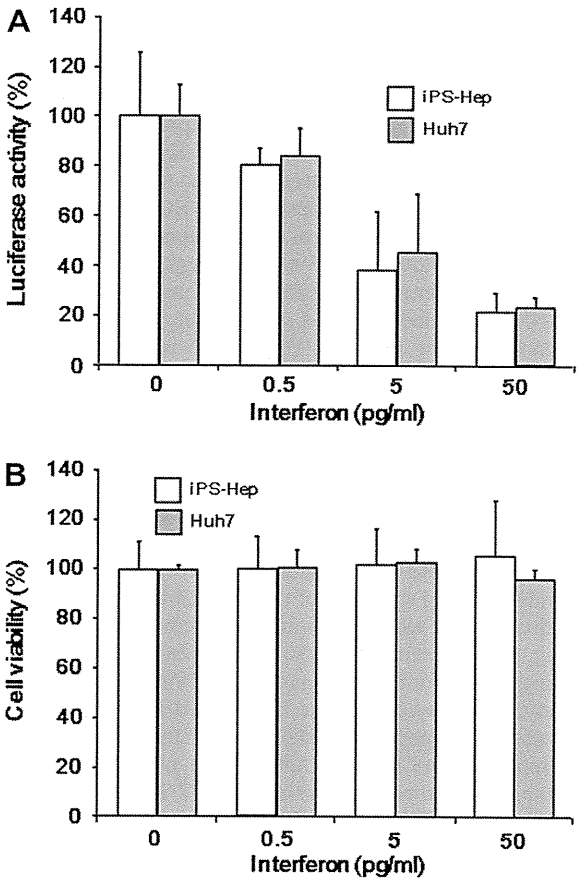

Fig. 3. Effect of interferon on HCV replication in iPS-Hep cells. iPS-Hep (open column) and Huh7 (gray column) cells were infected with AdP$_i$235-HCV and Ad-tTA. After 24 h, the cells were treated with Dox and the indicated concentration of interferon for 48 h. Luciferase activities (A) and cell viabilities (B) were measured as described in the Section 2. Data represent the percentage of the value for vehicle-treated cells, and are presented as means ± SD (n = 3).

4. Discussion

Tropism of HCV is limited to human and chimpanzee. Our understanding of HCV infection has been delayed by the lack of appropriate model systems. In the present study, we demonstrated that iPS-Hep cells are suitable *in vitro* models of hepatocytes for use in the study of HCV infection.

Other *in vitro* model systems of hepatocytes may not accurately reflect the biology of hepatocytes *in vivo*. For instance, expression profiles of mRNAs in embryonic stem (ES) cell-derived hepatocyte-like cells are different from those of primary human hepatocytes [31]. The development of efficient methods to differentiate stem cells into hepatocytes has been a critical issue in the application of stem cell technology to drug discovery. Recently, Mizuguchi and colleagues established efficient differentiation protocols for iPS cells by using adenoviral transfer of SOX17 [17], HEX [18], and HNF-4α [19] in addition to growth factors. Approximately 80% of the differentiated cells showed expression of hepatic-specific proteins, including cytochrome P-450s (CYP2D6, CYP3A4, and CYP7A1) [19]. The iPS-Hep cells were also used as a simple system to evaluate the hepatotoxicity of drugs that are metabolized into toxic substances by cytochromes [19]. Here, we showed that the essential host factors for HCV infection (occludin, claudin-1, SR-BI, and CD81) are expressed in the iPS-Hep cells. HCV RNA genome replication occurred in the cells, and HCVpv infected the cells. An inhibitor of HCV entry (anti-CD81 antibody), and an anti-HCV agent (IFN), attenuated the entry of HCVpv and the replication of the HCV genome in the cells, respectively. These findings suggest that the iPS-Hep cells are useful for understanding HCV infection and for screening anti-HCV drugs.

We found that iPS cells express CD81 and occludin, and are not susceptible to HCV entry, whereas iPS-Hep cells express all four HCV receptors and are susceptible to HCV entry. These findings are consistent with previous studies showing that CD81, occludin,

SR-BI, and claudin-1 are key receptors for HCV [29]. HNF-4α, which promotes the differentiation of iPS cells to iPS-Hep cells, is essential for the expression of a multitude of genes encoding cell junction and adhesion proteins during embryonic development of the mouse liver [32]. For instance, claudin-1 expression is not detected in the liver of HNF-4α-deficient mice [32]. HNF-4α enhances peroxisome proliferator-activated receptor-mediated SR-BI transcription [33]. Thus, the susceptibility to HCV entry observed in iPS-Hep cells may be the result of the additional expression of claudin-1 and SR-BI following HNF-4α treatment.

miR-122 is a liver specific miRNA that constitutes 70% of the total miRNA population [34] and is essential for replication of the HCV genome in the liver [6]. ES cells do not express miR-122, whereas expression of miRNA is observed during differentiation into hepatocyte-like cells [35]. Replication of HCV subgenomic replicons was observed in iPS-Hep cells, but not iPS cells (Fig. 2A). Expression of miR-122 might be a key factor controlling the replication of the HCV RNA genome in iPS-Hep cells.

The reasons that 15–20% of people infected with HCV can clear the virus without pharmaceutical intervention, and patients vary in their sensitivity to pharmaceutical treatments, are still unclear [36]. Understanding the basis of these variable responses to infection and treatment would facilitate the discovery of potent targets for drug development for HCV. iPS-derived hepatocytes are a promising system for drug discovery for HCV infection. In the present study, we showed that the iPS-derived hepatocyte-like cells can be used with popular models of HCV infection: HCV subgenomic replicons and HCVpv. Our findings will contribute to our understanding of the mechanisms of HCV infection and to the identification of novel targets for HCV therapy by means of iPS technology.

Acknowledgments

This work was supported by a Health and Labor Sciences Research Grant from the Ministry of Health, Labor and Welfare of Japan (HM, FS and KY), by a Grant-in-Aid for Scientific Research from the Ministry of Education, Culture, Sports, Science and Technology, Japan (23659039, MK) by the Japan Research Foundation for Clinical Pharmacology (HM), and by the Uehara Memorial Foundation (HM).

References

[1] S.A. Sarbah, Z.M. Younossi, Hepatitis C: an update on the silent epidemic, J. Clin. Gastroenterol. 30 (2000) 125–143.

[2] J. Schlutter, Therapeutics: new drugs hit the target, Nature 474 (2011) S5–7.

[3] N. Sakamoto, M. Watanabe, New therapeutic approaches to hepatitis C virus, J. Gastroenterol. 44 (2009) 643–649.

[4] N. Sakamoto, G.Y. Wu, Prospects for future therapy of hepatitis C virus infection, Future Virology 4 (2009) 453–462.

[5] C. Sarrazin, T.L. Kieffer, D. Bartels, B. Hanzelka, U. Muh, M. Welker, D. Wincheringer, Y. Zhou, H.M. Chu, C. Lin, C. Weegink, H. Reesink, S. Zeuzem, A.D. Kwong, Dynamic hepatitis C virus genotypic and phenotypic changes in patients treated with the protease inhibitor telaprevir, Gastroenterology 132 (2007) 1767–1777.

[6] C.L. Jopling, M. Yi, A.M. Lancaster, S.M. Lemon, P. Sarnow, Modulation of hepatitis C virus RNA abundance by a liver-specific microRNA, Science 309 (2005) 1577–1581.

[7] R.E. Lanford, E.S. Hildebrandt-Eriksen, A. Petri, R. Persson, M. Lindow, M.E. Munk, S. Kauppinen, H. Orum, Therapeutic silencing of microRNA-122 in primates with chronic hepatitis C virus infection, Science 327 (2010) 198–201.

[8] J. Lupberger, M.B. Zeisel, F. Xiao, C. Thumann, I. Fofana, L. Zona, C. Davis, C.J. Mee, M. Turek, S. Gorke, C. Royer, B. Fischer, M.N. Zahid, D. Lavillette, J. Fresquet, F.L. Cosset, S.M. Rothenberg, T. Pietschmann, A.H. Patel, P. Pessaux, M. Doffoel, W. Raffelsberger, O. Poch, J.A. McKeating, L. Brino, T.F. Baumert, EGFR and EphA2 are host factors for hepatitis C virus entry and possible targets for antiviral therapy, Nat. Med. 17 (2011) 589–595.

[9] J. Bukh, A critical role for the chimpanzee model in the study of hepatitis C, Hepatology 39 (2004) 1469–1475.

[10] K. Takahashi, K. Tanabe, M. Ohnuki, M. Narita, T. Ichisaka, K. Tomoda, S. Yamanaka, Induction of pluripotent stem cells from adult human fibroblasts by defined factors, Cell 131 (2007) 861–872.

[11] L.E. Greenbaum, From skin cells to hepatocytes: advances in application of iPS cell technology, J. Clin. Invest. 120 (2010) 3102–3105.

[12] E. Kiskinis, K. Eggan, Progress toward the clinical application of patient-specific pluripotent stem cells, J. Clin. Invest. 120 (2010) 51–59.

[13] H. Gai, D.M. Nguyen, Y.J. Moon, J.R. Aguila, L.M. Fink, D.C. Ward, Y. Ma, Generation of murine hepatic lineage cells from induced pluripotent stem cells, Differentiation 79 (2010) 171–181.

[14] K. Si-Tayeb, F.K. Noto, M. Nagaoka, J. Li, M.A. Battle, C. Duris, P.E. North, S. Dalton, S.A. Duncan, Highly efficient generation of human hepatocyte-like cells from induced pluripotent stem cells, Hepatology 51 (2010) 297–305.

[15] Z. Song, J. Cai, Y. Liu, D. Zhao, J. Yong, S. Duo, X. Song, Y. Guo, Y. Zhao, H. Qin, X. Yin, C. Wu, J. Che, S. Lu, M. Ding, H. Deng, Efficient generation of hepatocyte-like cells from human induced pluripotent stem cells, Cell Res. 19 (2009) 1233–1242.

[16] G.J. Sullivan, D.C. Hay, I.H. Park, J. Fletcher, Z. Hannoun, C.M. Payne, D. Dalgetty, J.R. Black, J.A. Ross, K. Samuel, G. Wang, G.Q. Daley, J.H. Lee, G.M. Church, S.J. Forbes, J.P. Iredale, I. Wilmut, Generation of functional human hepatic endoderm from human induced pluripotent stem cells, Hepatology 51 (2010) 329–335.

[17] K. Takayama, M. Inamura, K. Kawabata, K. Tashiro, K. Katayama, F. Sakurai, T. Hayakawa, M.K. Furue, H. Mizuguchi, Efficient and directive generation of two distinct endoderm lineages from human ESCs and iPSCs by differentiation stage-specific SOX17 transduction, PLoS One 6 (2011) e21780.

[18] M. Inamura, K. Kawabata, K. Takayama, K. Tashiro, F. Sakurai, K. Katayama, M. Toyoda, H. Akutsu, Y. Miyagawa, H. Okita, N. Kiyokawa, A. Umezawa, T. Hayakawa, M.K. Furue, H. Mizuguchi, Efficient generation of hepatoblasts from human ES cells and iPS cells by transient over-expression of homeobox gene HEX, Mol. Ther. 19 (2011) 400–407.

[19] K. Takayama, M. Inamura, K. Kawabata, K. Katayama, M. Higuchi, K. Tashiro, A. Nonaka, F. Sakurai, T. Hayakawa, M.K. Furue, H. Mizuguchi, Efficient generation of functional hepatocytes from human embryonic stem cells and induced pluripotent stem cells by HNF4α transduction, Mol. Ther. (in press).

[20] H. Makino, M. Toyoda, K. Matsumoto, H. Saito, K. Nishino, Y. Fukawatase, M. Machida, H. Akutsu, T. Uyama, Y. Miyagawa, H. Okita, N. Kiyokawa, T. Fujino, Y. Ishikawa, T. Nakamura, A. Umezawa, Mesenchymal to embryonic incomplete transition of human cells by chimeric OCT4/3 (POU5F1) with physiological co-activator EWS, Exp. Cell Res. 315 (2009) 2727–2740.

[21] S. Nagata, M. Toyoda, S. Yamaguchi, K. Hirano, H. Makino, K. Nishino, Y. Miyagawa, H. Okita, N. Kiyokawa, M. Nakagawa, S. Yamanaka, H. Akutsu, A. Umezawa, T. Tada, Efficient reprogramming of human and mouse primary extra-embryonic cells to pluripotent stem cells, Genes Cells 14 (2009) 1395–1404.

[22] M.K. Furue, J. Na, J.P. Jackson, T. Okamoto, M. Jones, D. Baker, R. Hata, H.D. Moore, J.D. Sato, P.W. Andrews, Heparin promotes the growth of human embryonic stem cells in a defined serum-free medium, Proc. Natl. Acad. Sci. USA 105 (2008) 13409–13414.

[23] H. Tani, Y. Komoda, E. Matsuo, K. Suzuki, I. Hamamoto, T. Yamashita, K. Moriishi, K. Fujiyama, T. Kanto, N. Hayashi, A. Owsianka, A.H. Patel, M.A. Whitt, Y. Matsuura, Replication-competent recombinant vesicular stomatitis virus encoding hepatitis C virus envelope proteins, J. Virol. 81 (9) (2007) 8601–8612.

[24] T. Yoshida, M. Kondoh, M. Ojima, H. Mizuguchi, Y. Yamagishi, N. Sakamoto, K. Yagi, Adenovirus vector-mediated assay system for hepatitis C virus replication, Nucleic Acids Res. 39 (2011) e64.

[25] H. Mizuguchi, T. Hayakawa, Characteristics of adenovirus-mediated tetracycline-controllable expression system, Biochim. Biophys. Acta 1568 (2002) 21–29.

[26] H. Mizuguchi, M.A. Kay, Efficient construction of a recombinant adenovirus vector by an improved *in vitro* ligation method, Hum. Gene Ther. 9 (1998) 2577–2583.

[27] N.C. Besnard, P.M. Andre, Automated quantitative determination of hepatitis C virus viremia by reverse transcription-PCR, J. Clin. Microbiol. 32 (1994) 1887–1893.

[28] F. Komurian-Pradel, M. Perret, B. Deiman, M. Sodoyer, V. Lotteau, G. Paranhos-Baccala, P. Andre, Strand specific quantitative real-time PCR to study replication of hepatitis C virus genome, J. Virol. Methods 116 (2004) 103–106.

[29] M.B. Zeisel, I. Fofana, S. Fafi-Kremer, T.F. Baumert, Hepatitis C virus entry into hepatocytes: molecular mechanisms and targets for antiviral therapies, J. Hepatol. 54 (2011) 566–576.

[30] K. Moriishi, Y. Matsuura, Evaluation systems for anti-HCV drugs, Adv. Drug Deliv. Rev. 59 (2007) 1213–1221.

[31] M. Ek, T. Soderdahl, B. Kuppers-Munther, J. Edsbagge, T.B. Andersson, P. Bjorquist, I. Cotgreave, B. Jernstrom, M. Ingelman-Sundberg, I. Johansson, Expression of drug metabolizing enzymes in hepatocyte-like cells derived from human embryonic stem cells, Biochem. Pharmacol. 74 (2007) 496–503.

[32] M.A. Battle, G. Konopka, F. Parviz, A.L. Gaggl, C. Yang, F.M. Sladek, S.A. Duncan, Hepatocyte nuclear factor 4alpha orchestrates expression of cell adhesion proteins during the epithelial transformation of the developing liver, Proc. Natl. Acad. Sci. USA 103 (2006) 8419–8424.

[33] L. Malerod, M. Sporstol, L.K. Juvet, A. Mousavi, T. Gjoen, T. Berg, Hepatic scavenger receptor class B, type I is stimulated by peroxisome proliferator-

activated receptor gamma and hepatocyte nuclear factor 4alpha, Biochem. Biophys. Res. Commun. 305 (2003) 557–565.
[34] M. Lagos-Quintana, R. Rauhut, A. Yalcin, J. Meyer, W. Lendeckel, T. Tuschl, Identification of tissue-specific microRNAs from mouse, Curr. Biol. 12 (2002) 735–739.
[35] N. Kim, H. Kim, I. Jung, Y. Kim, D. Kim, Y.M. Han, Expression profiles of miRNAs in human embryonic stem cells during hepatocyte differentiation, Hepatol. Res. 41 (2011) 170–183.
[36] L. Gravitz, A. Smouldering, Public-health crisis, Nature 474 (2011) S2–S4.

Biomaterials 33 (2012) 3464–3474

Contents lists available at SciVerse ScienceDirect

Biomaterials

journal homepage: www.elsevier.com/locate/biomaterials

Creation and biochemical analysis of a broad-specific claudin binder

Azusa Takahashi [a,1], Yumiko Saito [a,1], Masuo Kondoh [a,*,1], Kyohei Matsushita [a], Susanne M. Krug [b], Hidehiko Suzuki [a], Hirofumi Tsujino [c], Xiangru Li [a], Hiroshi Aoyama [c], Koji Matsuhisa [a], Tadayuki Uno [c], Michael Fromm [b], Takao Hamakubo [d], Kiyohito Yagi [a]

[a] Laboratory of Bio-Functional Molecular Chemistry, Graduate School of Pharmaceutical Sciences, Osaka University, Suita, Osaka 565-0871, Japan
[b] Institute of Clinical Physiology, Charite, Campus Benjamin Franklin, Freie University and Humboldt University, Berlin, Germany
[c] Laboratory of Analytical Chemistry, Graduate School of Pharmaceutical Sciences, Osaka University, Suita, Osaka 565-0871, Japan
[d] Department of Molecular Biology and Medicine, Research Center for Advanced Science and Technology, The University of Tokyo, Meguro, Tokyo 153-8904, Japan

ARTICLE INFO

Article history:
Received 26 December 2011
Accepted 9 January 2012
Available online 7 February 2012

Keywords:
Claudin
Drug delivery system
Baculovirus
Phage display
Tight junction

ABSTRACT

Claudins (CL) are a family of tetra-transmembrane proteins that are the structural and functional components of tight junctions (TJ). CLs are promising targets for drug development because of their role in mucosal drug absorption and cancer. However, CL-targeted drug development has been delayed because CLs have low antigenicity and preparing CL proteins is difficult. We developed a CL binder by using the C-terminal fragment of *Clostridium perfringens* enterotoxin (C-CPE) and a baculoviral display system. After screening CL binders from a C-CPE mutant-displaying library by using CL-displaying budded baculovirus (BV) we isolated a C-CPE mutant called m19, which bound to CL1, CL2, CL4 and CL5. A 3-dimensional analysis showed that m19 has a structural backbone similar to C-CPE. The charge density of the CL-binding domains of m19 and C-CPE differed, suggesting that electrostatic interactions may occur between m19 and CLs. Treatment of epithelial cells with m19 decreased the paracellular but not transcellular integrity, and m19 enhanced jejunal absorption. Thus, we successfully created a CL binder with broad specificity. These findings will contribute to future preparation of CL binders for CL-targeted drug development.

1. Introduction

Epithelia covers the body surface and prevents entry of xenobiotics and pathogens into the body. The most critical role of epithelium is to form a barrier separating the body from the environment. Tight junctions (TJs) are located in the apical part of the lateral membranes and seal the intercellular space to prevent free movement of solutes via the paracellular spaces by forming points of fusion between the membranes [1].

Modulation of TJ-seals has been investigated as a strategy to improve drug absorption [2]. Most malignant tumors are derived from epithelium. The early stages of cancer are frequently associated with the loss of intercellular adhesion and cellular polarity [3]. Mucosal vaccination is a promising therapy for infectious diseases [4]. Many studies have investigated the efficient delivery of antigens to mucosal immune tissues in epithelium [5,6]. Therefore, epithelia are promising therapeutic targets for drug absorption, infectious diseases, and cancer.

A series of biochemical analyses of TJs revealed that intercellular TJ-seals contains transmembrane proteins, such as occludin, tricellulin, the family of claudin (CL) and junction adhesion molecule [7]. CLs are estimated to be the primary structural and functional components of the TJ-seal. Mammalian CLs are a family of 27 known tetra-transmembrane proteins [8,9]. CLs form homo- and hetero-type strands on the cell membrane, and adjacent CL strands interact with those on the lateral membrane, leading to the formation of TJ-seals [10]. The properties of the TJ-barrier are determined by a combination of CL proteins. CL1- and CL5-deficient mice show disruption of the epidermal barrier and the blood–brain barrier, respectively [11,12]. Some malignant tumors, including

Abbreviations: CL, claudin; TJ, tight junction; C-CPE, C-terminal fragment of *Clostridium perfringens* enterotoxin; BV, budded baculovirus; CPE, *Clostridium perfringens* enterotoxin; TBS, Tris-buffered saline; SDS-PAGE, sodium dodecyl sulfate-polyacrylamide gel electrophoresis; PCR, polymerase chain reaction; PBS, phosphate-buffered saline; ELISA, enzyme-linked immunosorbent assay; FACS, fluorescence activated cell sorting; TEER, transepithelial electrical resistance; FD-4, fluorescein isothiocyanate-labeled dextran with a molecular mass of 4 kDa; AUC, area under the curve.

* Corresponding author. Laboratory of Bio-Functional Molecular Chemistry, Graduate School of Pharmaceutical Sciences, Osaka University, Suita, Osaka 565-0871, Japan. Tel.: +81 6 6879 8196; fax: +81 6 6879 8199.
E-mail address: masuo@phs.osaka-u.ac.jp (M. Kondoh).

[1] These authors equally contributed to this study.

0142-9612/$ – see front matter © 2012 Elsevier Ltd. All rights reserved.
doi:10.1016/j.biomaterials.2012.01.017

pancreatic, breast and lung cancers overexpress CLs [13]. Epithelial cells covering mucosal immune tissues express CL4 [14,15]. CL1 is a co-receptor for hepatitis C virus [16]. These findings strongly indicate that CLs may be a strong candidate for epithelium-targeted drug development. However, CLs have low antigenicity and preparing CL proteins is difficult, so that the development of CLs binders has been slow.

Clostridium perfringens enterotoxin (CPE), a 35-kDa polypeptide, is a food poison that is lethal to humans [17]. CPE has an N-terminal cytotoxic domain and a C-terminal receptor binding domain (C-CPE) [18,19]. The CPE receptors are identical to those on CL3 and CL4 [18,20]. C-CPE contains 184-319 amino acids and was the only known nontoxic CL3/4 binder before 2005 [20]. CPE has high affinity to CL3 and CL4 with a Ka value of approximately $1.0 \times 10^8\ M^{-1}$ [21]. Modulation of TJ-barriers by using the CL binders C-CPE and part of the N-terminally truncated mutants enhances jejunal, nasal and pulmonary absorption of drugs [22,23]. We prepared CL binders fused to protein synthesis inhibitory factor derived from *Pseudomonas aeruginosa* exotoxin, and found that a CL-targeting toxin showed antitumor activity [24–26]. C-CPEs were used to develop an efficient system to deliver antigen to mucosal immune tissue [27]. CPE shows antitumor activity against brain and pancreatic tumors with no apparent side effects [28,29]. These findings indicate that ligands for CLs may be promising molecules for drug development.

We previously determined the functional domain of the C-CPEs, and prepared a phage library displaying C-CPE mutants, in which the functional amino acid residues were randomly altered [30–32]. Developing a screening system for CL binders was necessary because it is difficult to prepare CL proteins. Budded baculovirus (BV) displays membrane proteins on its surface in an active form [33,34], and we already found that CL-displaying BV provides a screen for CL binders [30]. In the present study, we screened CL binders from the C-CPE mutant library by using CL-displaying BV.

2. Materials and methods

2.1. Cell culture

A mouse fibroblast cell line (L cells) and mouse CL1, CL2, CL4 or CL5-expressing L cells (CL1/L cells, CL2/L cells, CL4/L cells, CL5/L cells) were kindly provided by Dr. S. Tsukita (Kyoto University, Kyoto, Japan). Sf9 cells and Caco-2 cells were obtained from Invitrogen (Gaithersburg, MD) and ATCC cell bank (Manassas, VA), respectively. L cells were maintained in modified Eagle's medium supplemented with 10% fetal bovine serum (FBS) in a 5% CO_2 atmosphere at 37 °C. Huh7 cells were cultured in Dulbecco's modified Eagle's medium (DMEM) supplemented with 10% FBS. The cells were maintained in a 5% CO_2 atmosphere at 37 °C. Mock or bicellularly tricellulin-overexpressing MDCK II cells (MDCK V1 or MDCK TRa-8) were maintained in DMEM supplemented with 400 μg/ml G418, 10% FBS, 100 μg/ml streptomycin (Invitrogen) [35].

2.2. Recombinant BV construction and Sf9 cell culture

Mouse CL1, CL4 and CL5 cDNAs were kindly provided by Dr. M. Furuse (Kobe University, Japan). Recombinant BV was prepared by using the Bac-to-Bac expression system, according to the manufacturer's instructions (Invitrogen). Briefly, CL cDNA were inserted into pFastBac1, and the resulting plasmids were transduced into DH10Bac *E. coli* cells. Recombinant bacmid DNA was extracted from the cells. Sf9 cells were transduced with the bacmid encoding CL, and the recombinant BV was recovered by centrifugation of the conditioned medium [25].

2.3. Preparation of the BV fractions

Sf9 cells (2×10^6 cells) were infected with recombinant BV at a multiplicity of infection of 5. The BV fraction was recovered from the culture supernatant of infected Sf9 cells by centrifugation 72 h after infection. The pellets of the BV fraction were resuspended in Tris-buffered saline (TBS) containing 1% protease inhibitor cocktail (Sigma-Aldrich, St. Louis, MO) and stored at 4 °C until used. The expression of CL1 and CL4 in the BV was confirmed by sodium dodecyl sulfate-polyacrylamide gel electrophoresis (SDS-PAGE) and an immunoblot analysis with anti-CL antibodies (Invitrogen).

2.4. Preparation of mutant C-CPE library

A C-CPE mutant-displaying phage library was prepared as described previously [30]. Briefly, C-CPE fragments in which the functional amino acids (S304, S305, S307, N309, S313 and K318) [31] were randomly mutated were prepared by PCR with pET-H_{10}PER as a template and primers with triplet codons coding the functional amino acids randomly changed to triplet codons coding any of the 20 amino acids. The PCR fragments were inserted into a phagemid. The resultant phagemid containing the C-CPE mutant library was transduced into *E. coli* TG1 cells, and the cells were stored at −80 °C.

2.5. Preparation of phage

TG1 cells containing the phagemid coding C-CPE mutant library were cultured in 2YT medium (Invitrogen) containing 2% glucose and ampicillin. M13K07 helper phages (Invitrogen) were added when the cells reached the growth phase, and the medium was changed to 2YT medium containing ampicillin and kanamycin. The cells were cultured an additional 6 h and the phages in the conditioned medium were precipitated with polyethylene glycol. The phages were suspended in NTE buffer (100 mM NaCl, 10 mM Tris, 1 mM EDTA) and stored at 4 °C until use.

2.6. Screening of phages using BV

CL1-BVs (0.5 μg protein) were adsorbed onto an immunotube (Nunc, Roskilde, Denmark). The C-CPE phage library was transferred to the BV-coated tubes, and the tubes were washed 15 times with phosphate-buffered saline (PBS) containing 0.05% Tween 20. The phages bound to the tube were eluted with 100 mM HCl. TG1 cells were infected with the eluted phages; the phages had been prepared as described above. The resulting phages were subjected to repeated selection using the CL1-BV-coated immunotubes. We performed sequencing analysis with a 5′-gtaaat-gaattttctgtatgagg-3′ primer to identify the isolated phage clones.

2.7. Measurement of phage titer

We measured the titer (colony formation unit (CFU)/ml) of the phage solution to quantify the concentration of phages. Briefly, the phage solution was diluted to 10^{-5}–10^{-10} with 2YT containing 2% glucose. The diluted solution was infected with TG1 cells, and the cells were seeded onto Petrifilm™ (Tech-Jam, Osaka, Japan). The colonies were counted after 16 h of incubation, and the titer was calculated.

2.8. Purification of C-CPE mutants

The plasmids containing C-CPE mutants derived from the CL1-bound phage clones were prepared by PCR-amplifying the C-CPE mutant fragments with the phagemid coding C-CPE mutants as template, a common forward primer (5′-ggaattccatatggatatagaaaaagaaatccttgatttagctg-3′, the *NdeI* site is underlined), and a reverse primer for C-CPE mutants (5′-cgcggatcc<u>ttaaaacttttgaaataatat</u>-3′, the *BamHI* site is underlined). The site-directed C-CPE mutant fragments were cloned by PCR with C-CPE or C-CPE mutants as template. The resulting PCR fragment was inserted into pET16b, and the sequence was confirmed. The plasmids were transduced into *E. coli* strain BL21 (DE3), and production of mutant C-CPEs was induced by the addition of isopropyl-D-thiogalactopyranoside. The harvested cells were lysed in buffer A (10 mM Tris-HCl, pH 8.0, 400 mM NaCl, 5 mM $MgCl_2$, 0.1 mM phenylmethanesulfonyl fluoride, 1 mM 2-mercaptoethanol, and 10% glycerol). The lysates were applied to HiTrap™ Chelating HP (GE Healthcare, Buckinghamshire, UK), and mutant C-CPEs were eluted with buffer A containing imidazole. The buffer was exchanged with PBS by using a PD-10 column (GE Healthcare), and the purified protein was stored at −80 °C until used. Purification of the mutant C-CPEs was confirmed by SDS-PAGE, followed by staining with Coomassie Brilliant Blue. Protein was quantified with a BCA protein assay kit with bovine serum albumin as standard (Pierce Chemical, Rockford, IL).

2.9. Enzyme-linked immunosorbent assay (ELISA)

The BV-displaying CLs were diluted with TBS and adsorbed to the wells of 96-well immunoplates (Nunc, Roskilde, Denmark) overnight at 4 °C. The wells were washed with PBS and blocked with TBS containing 4% BlockAce (Dainippon Sumitomo Pharma, Osaka, Japan) for 2 h at room temperature. The phages or C-CPEs were added to the well and incubated for an additional 2 h at room temperature. The wells were washed with PBS and incubated with anti-M13 antibody or anti-His-tag antibody for 2 h at room temperature. The immunoreactive proteins were detected by an HRP-labeled secondary antibody with 3,3′,5,5′-tetramethylbenzine as substrate. The reaction was terminated by the addition of 1 M H_2SO_4, and the optical density of the immunoreactive proteins were measured at 450 nm.

2.10. Fluorescence-activated cell sorting

The CLs/L cells were incubated with C-CPEs for 1 h at 4 °C, followed by incubation with an anti C-CPEs-fused tag antibody. The cells were incubated

with fluorescein-labeled secondary antibody, and the C-CPEs-bound cells were detected and analyzed with a flow cytometer (FACScalibur, Becton Dickinson, New Jersey, USA).

2.11. Crystallization

Initial screening of crystallization conditions was performed by sitting drop vapor diffusion using the JBScreen Crystal Screening Kit (Jena Bioscience GmbH, Jena, Germany) by mixing equal volumes of m19 and well solution. Drops were equilibrated against the well solution at 25 °C. The crystals used in the analysis were obtained by mixing 1 μl of protein solution at 9 mg/ml, 1 μl of reservoir solution containing 0.1 M sodium acetate, pH 4.6 and 1.75 M ammonium sulfate, and allowing the drop to equilibrate against 1 ml of reservoir solution by the hanging drop method.

2.12. Data collection, phasing, and refinement

X-ray diffraction data on the m19 crystals were collected at 100 K in a nitrogen stream, after the crystals were soaked with 3.4 M sodium malonate pH 5.0 as a cryoprotectant. X-ray data were collected from a single crystal at 2.0 Å with a Raynoix MX225HE CCD detector on the beamline BL44XU at SPring-8 (Table 1). The x-ray wavelength was 0.9 Å, the angle oscillation range was 1.0, and the crystal-to detector distance was 230 mm.

The diffraction data were processed using the programs iMOSFLM [36] and SCALA [37] from the CCP4 suite [38]. m19 structure was solved by molecular replacement method using the program BALBES [39] and the atomic coordinates of C-CPE (PDB ID : 2QUO). The model was examined and manually fitted based on the 2Fo − Fc and Fo − Fc electron density maps using the program COOT [40]. Isotropic restrained refinement was performed using the program REFMAC5 [41]. Data collection and refinement statistics are shown in Table 1.

2.13. Transepithelial electrical resistance (TEER)

Caco-2 cells were seeded in BD BioCoat™ Fibrillar Collagen Cell Culture Inserts (BD Biosciences, Franklin Lakes, NJ) at a subconfluent density. The TEER of the Caco-2 monolayer cell sheets on the chamber was monitored using a Millicell-ERS epithelial volt-ohmmeter (Millipore, Billerica, MA). The Caco-2 monolayers were cultured for 5 days, and then treated with C-CPE or C-CPE mutants on the basal side of the insert. Changes in TEER values were monitored. The TEER values were normalized by the area of the Caco-2 monolayer, and the TEER value of a blank Transwell™ chamber (background) was subtracted.

Table 1
Data collection and refinement statistics.

Synchrotron/beamline	SPring-8/BL44XU
Crystal parameters	
Space Group	$P\,3_1\,2\,1$
Cell dimensions (Å)	$a = b = 87.63$, $c = 63.9$
Angles (°)	$\alpha = \beta = 90$, $\gamma = 120$
Data collection	
Wavelength (Å)	0.9
Resolution limit (Å)	37.94–2.00 (2.10–2.00)
R_{merge}	0.082 (0.962)
Total number of observations	213,338 (30,794)
Total number of unique	19,504 (2,827)
Observations	
Mean $I/\sigma I$	14.8 (2.5)
Completeness	99.4 (100.0)
Multiplicity	10.9 (10.9)
Refinement	
Protein atoms in model	989
Solvent atoms in model	66
$R_{working}$	0.233
R_{free}	0.252
Rmsd from ideal geometry	
Bond length (Å)	0.025
Bond angles (°)	2.315
Ramachandran plot (%)	
Most favored	95.9
Outlier	4.1

Values for the outermost resolution shell are given in parentheses.
$R_{merge} = \sum_{hkl} \sum_i |I_i(hkl) - \{I(hkl)\}| / \sum_{hkl} \sum_i I_i(hkl)$, where $I_i(hkl)$ is the intensity of the ith observation of reflection hkl and $\{I(hkl)\}$ is the average over all observations of reflection hkl.
$R_{working} = \sum_{hkl} || F_{obs}| - |F_{calc}|| / \sum_{hkl} |F_{obs}|$, where F_{obs} and F_{calc} are the observed and calculated structure-factor amplitudes, respectively.
R_{free} is $R_{working}$ calculated using 5% of the date that were omitted from refinement.

MDCK V1 or MDCK TRa-8 cells were seeded on porous polycarbonate microwell inserts (Millicell-HA, Millipore; 0.6-cm^2 area) and were grown to confluence. After 4 days, the cells were treated with C-CPE or C-CPE mutants on the basal side of the insert. TEER were determined before and 2 h after addition of C-CPEs. Values were normalized and background was subtracted.

2.14. Two-path impedance spectroscopy

Two-path impedance spectroscopy was performed as described previously [42]. Briefly, this method is based on a model describing the epithelial resistance, R^{epi}, as a parallel circuit consisting of the transcellular resistance, R^{trans}, and the paracellular resistance, R^{para}. The subepithelial resistance, R^{sub}, is in series to R^{epi} and here is caused by the filter support. The apical and the basolateral membranes of the confluent cell layer are represented by resistors and capacitors in parallel (R^a, C^a, and R^b, C^b, respectively). R^a and R^b add up to R^{trans}. A spectrum of alternating currents was applied (35 μA/cm^2, frequency range 1.3–65 kHz), and changes in tissue voltage were detected by phase-sensitive amplifiers (402 frequency response analyzer, Beran Instruments, Gilching, Germany; 1286 electrochemical interface; Solartron Schlumberger, Farnborough, United Kingdom). Complex impedance values (Z_{real}, $Z_{imaginary}$) were calculated and plotted in a Nyquist diagram. R^{trans} and R^{para} were determined from experiments in which impedance spectra and fluxes of fluorescein as a paracellular marker substance were obtained before and after chelating extracellular Ca^{2+} with EGTA. This caused TJs to partially open and to increase fluorescein flux. In separate experiments it has been demonstrated that changes of fluorescein fluxes are inversely proportional to R^{epi} changes (data not shown)

2.15. Immunohistochemistry and confocal fluorescence microscopy

After cells were grown to confluence on on porous polycarbonate microwell inserts (Millicell-HA, Millipore) and treated with C-CPE or m19 as described above. The inserts were rinsed with PBS, and fixed with methanol they were permeabilized with PBS containing 0.5% (vol/vol) Triton X-100. Primary antibodies were diluted: mouse anti-FLAG-M2 (Sigma-Aldrich) 1:500; rabbit anti-occludin (Invitrogen) 1:200; guinea pig anti-tricellulin 1:1000; Alexa Fluor 488 goat anti-guinea pig (Pineda-Antikörper-Service, Berlin, Germany [35]), 1:2000; secondary antibodies were: Alexa Fluor 488 goat anti-mouse; Alexa Fluor 594 goat anti-rabbit, 1:500 (Molecular Probes, Hamburg, Germany; MoBiTec). Immunofluorescence images were obtained with a confocal laser scanning microscope (LSM 510 Meta, Carl Zeiss, Jena, Germany), using excitation wavelengths of 543 and 488 nm.

2.16. Flux measurements of fluorescein isothiocyanate-dextran (FD-4)

All flux studies were performed in Ussing chambers under short-circuit conditions. For FD-4 fluxes, Ussing chambers were filled with 10 ml Ringer's per side, 50 μl of pre-dialyzed FD-4 (molecular mass ~4 kDa, 20 mM) were added apically, and basolateral samples (300 μl) were replaced with fresh Ringer's 0, 15, 30, 45, and 60 min after addition. Samples were analyzed with a fluorometer (Spectramax Gemini, Molecular devices) at 520 nm (fluorescein). Fluxes were calculated as increase in tracer quantity (corrected for dilution) per time unit and filter area (0.6 cm^2). Permeabilities were calculated as flux/concentration on the donor side.

2.17. In situ loop assay

Jejunal absorption of FD-4 was evaluated using an *in situ* loop assay as described previously [23]. The experiments were performed according to the guidelines of the Ethics Committee of Osaka University. Eight-week-old Wistar male rats were anesthetized with pentobarbital, a midline abdominal incision was

Table 2
Sequences of CL1-binding phage clones.

	304	305	307	309	313	318
C-CPE	Ser	Ser	Ser	Asn	Ser	Lys
m5	Arg	Ala	Pro	Arg	His	Asn
m9	Arg	Arg	Arg	Arg	Arg	Lys
m10	Arg	Ser	Ala	Arg	Lys	Lys
m11	Arg	Val	Arg	Arg	Arg	Lys
m17	Leu	Pro	Arg	Arg	Lys	Gln
m19	Ala	Pro	Arg	His	His	Lys
m21	Ala	Pro	Arg	Asp	Arg	Lys
m24	Arg	Arg	Gln	Gln	Arg	Lys
m36	Arg	Pro	Arg	Arg	His	Lys
m37	Arg	Pro	Arg	Phe	His	Gln
m86	Thr	Pro	Arg	Arg	His	Lys
m89	Ala	Pro	Arg	Ala	Arg	Thr

The top row shows the sequences of the randomly mutated amino acids of C-CPE. The left-most column is the clone numbers of the CL1-bound phages.

made, and the jejunum was washed with PBS. A 5-cm long jejunal loop was prepared by closing both ends with sutures. A mixture of FD-4 (2 mg) and C-CPEs was injected into the jejunal loop. Blood was collected from the jugular vein at the indicated time points. The plasma levels of FD-4 were measured with a fluorescence spectrophotometer (Tristar LBP941; Berthold Technologies, Bad Wildbad, Germany). The AUC of FD-4 from 0 to 6 h ($AUC_{0-6\ h}$) was calculated by the trapezoidal method.

3. Results

3.1. Screening of CL1 binders from the C-CPE mutant library

CL1 is a promising target for modulation of the mucosal and epidermal barrier, and cancer-targeting [11,13,43–45]. Therefore, we attempted to screen CL1 binders by using a C-CPE mutant-displaying phage library and CL1-BV. We prepared CL1-BV (Suppl. Fig. 1A). The C-CPE library was added to CL1-BV-adsorbed tubes, and the CL1-BV-bound phages were recovered (1st screening). We repeated this screening process two more times (2nd and 3rd screening). The ratio of the incubated phage titers to the recovered phage titers, measured to determine the enrichment of CL1-bound phages, increased during screening from 0.172×10^{-6} to 2.69×10^{-6}, indicating the efficiency of our screening system for CL1 binders (Suppl. Fig. 1B). We isolated CL1-binding phage clones after the 3rd screening, and investigated the interaction of each monoclonal phage with CL1-BV (Suppl. Fig. 1C).

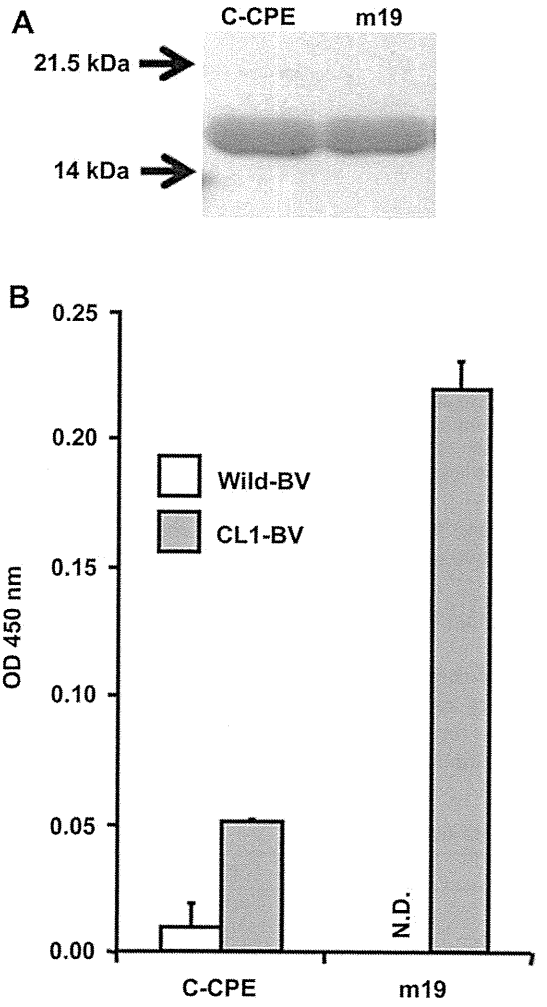

Fig. 1. Interaction of C-CPE mutants with CL1-BV. A) Purification of m19. m19 was expressed in *E. coli* and isolated by nickel-affinity chromatography. The purification of proteins was confirmed by SDS-PAGE. The putative molecular mass of C-CPEs is approximately 15 kDa. B) Interaction of m19 with CL1. m19 (2.0 μg) was added to wild-BV- or CL1-BV-coated immunoplates, followed by detection of C-CPE mutants bound to each type of BV. Data are presented as means ± SD ($n = 3$). N.D., not detected.

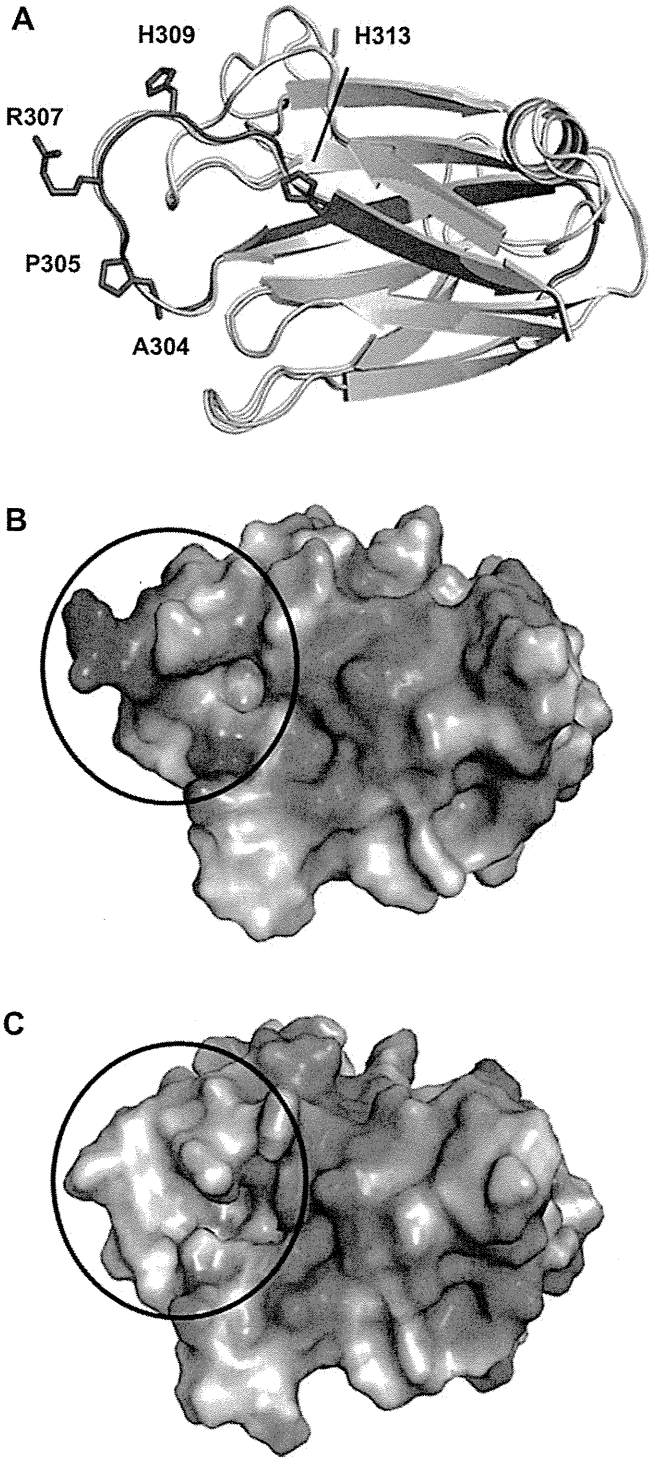

Fig. 2. The structure of m19. A) Superpositioning of m19 structure (yellow) on C-CPE (gray, PDB ID code 2QUO). The Cα rmsd for the superposition is 1.61 Å. The COOH-terminal 30 residues of m19, including β8 and β9 sheets and the intervening surface loop, are shown dark red. The mutated residues of m19 are shown as stick model. B, C) Electrostatic potential surface of m19 (B) and C-CPE (C). The color red, white, and blue indicate negative, neutral and positive charges, respectively. The circle indicates the putative CL-binding region [47].

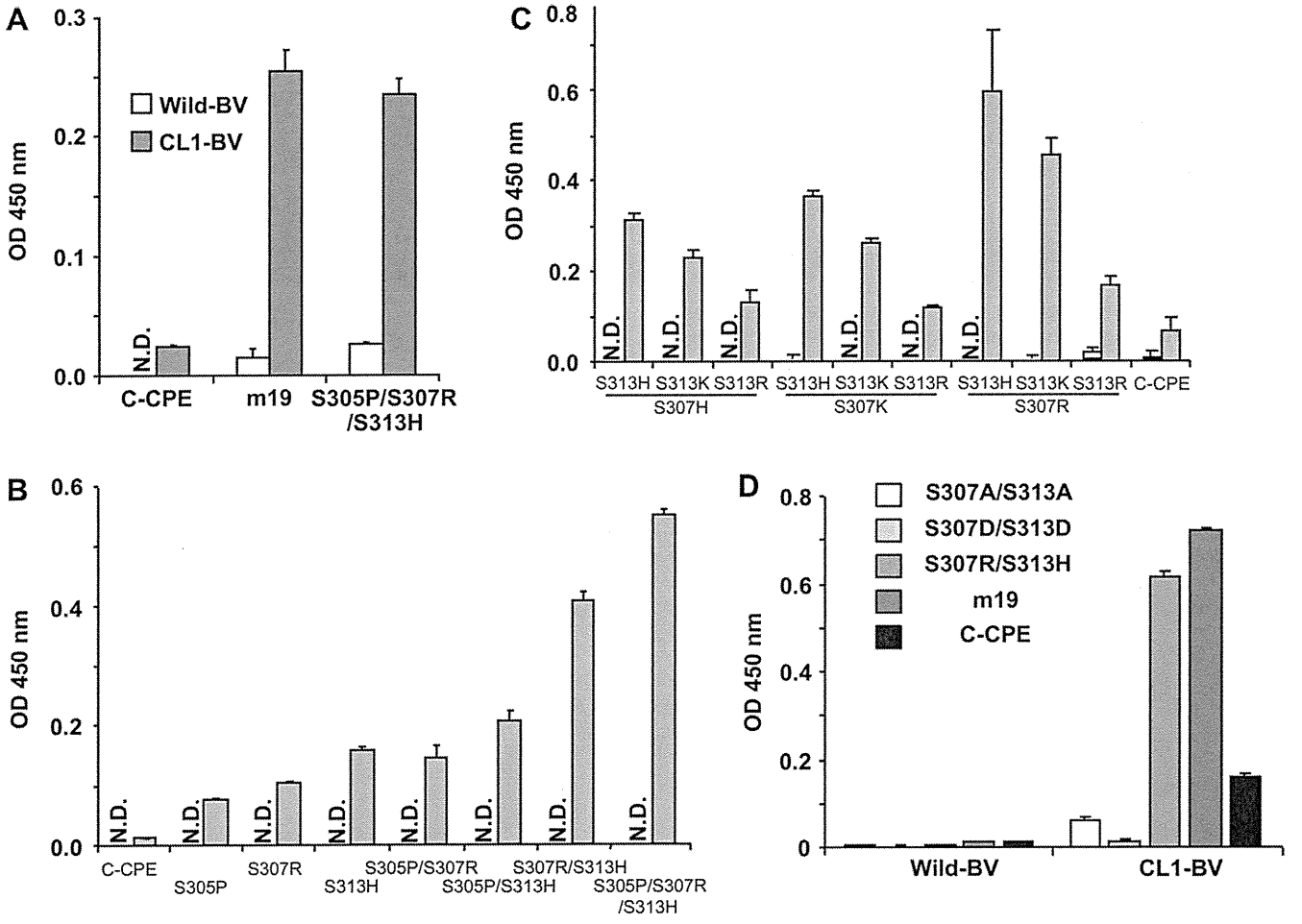

Fig. 3. Identification of the functional amino acids associated with CL1-binding to m19. A) Interaction of C-CPE, m19, or triple mutated C-CPE with CL1. C-CPE, m19 or the triple mutated C-CPE (2.0 μg) was added to wild-BV- or CL1-BV-coated immunoplates, followed by detection of binding to each type of BV. Data are presented as means ± SD ($n = 3$). B) Interaction of C-CPE or single or double-substituted C-CPE mutants with CL1. C-CPE or C-CPE mutants (2.0 μg) were added to wild-BV- or CL1-BV-coated immunoplates, followed by detection of binding to each type of BV. Data are presented as means ± SD ($n = 3$). C) Effects of a positive charge in C-CPE at positions 307 and 313 on interaction between C-CPE mutants and CL1-BV. C-CPE or C-CPE mutants (2.0 μg) was added to wild-BV- or CL1-BV-coated immunoplates, followed by detection of binding to each type of BV. Data are presented as means ± SD ($n = 3$). N.D., not detected. D) Effects of a negative charge in C-CPE at positions 307 and 313 on interaction between C-CPE mutants and CL1-BV. C-CPE or C-CPE mutants (2.0 μg) were added to wild-BV- or CL1-BV-coated immunoplates, followed by detection of binding to each type of BV. Data are presented as means ± SD ($n = 3$).

We analyzed the sequences of the CL1-BV-bound phages and identified CL1-binder candidates with amino acid sequences that differed from the wild-type sequence (Table 2). We prepared the recombinant proteins and investigated their interaction with CL1 by ELISA with CL-BVs (Fig. 1). m19, m36 and m86 were CL1 binders (data not shown on m36 and m86).

3.2. Structure of m19

We determined the three-dimensional structure of m19 to clarify why m19 bound to CL1. The structure of m19 was solved to a resolution of 2.00 Å by using molecular replacement method using the atomic coordinates of C-CPE (PDB ID : 2QUO). The final model has good stereochemistry and an R_{free} of 25.2%. A full summary of the data and refinement statistics is included in Table 1.

m19 has a structural backbone that is similar to C-CPE (Fig. 2A). Each protein contains 9 β-sheets and one α-helix. The loop domain between the β 8- and β 9-sheets is the putative CL binding domain [46]. Their loop domains have the same backbone (Fig. 2A). In contrast, the electrostatic map of the binding pocket region differed between C-CPE and m19 (Fig. 2B). The substitution of Ser with Ala, Ser with Pro, Ser with Arg, Asn with His and Ser with His at positions 304, 305, 307, 309 and 313, respectively, resulted in a more positive charge in the putative CL binding domain.

3.3. Functional domain mapping of m19

There are three common substitutions among m19, m36 and m86: Pro, Arg and His replaced Ser at positions 305, 307 and 313, respectively (Table 2), indicating that these substitutions may be involved in binding of the C-CPE mutants to CL1. We prepared

Table 3
Sequences of m19 mutants.

	304	305	307	309	313	318
C-CPE	Ser	Ser	Ser	Asn	Ser	Lys
m19	Ala	Pro	Arg	His	His	Lys
Triple mutant	Ser	Pro	Arg	Asn	His	Lys
S305P	Ser	Pro	Ser	Asn	Ser	Lys
S307R	Ser	Ser	Arg	Asn	Ser	Lys
S313H	Ser	Ser	Ser	Asn	His	Lys
S305P/S307R	Ser	Pro	Arg	Asn	Ser	Lys
S305P/S313H	Ser	Pro	Ser	Asn	His	Lys
S307R/S313H	Ser	Ser	Arg	Asn	His	Lys

We prepared C-CPE mutants that contained single or double substituted amino acids.

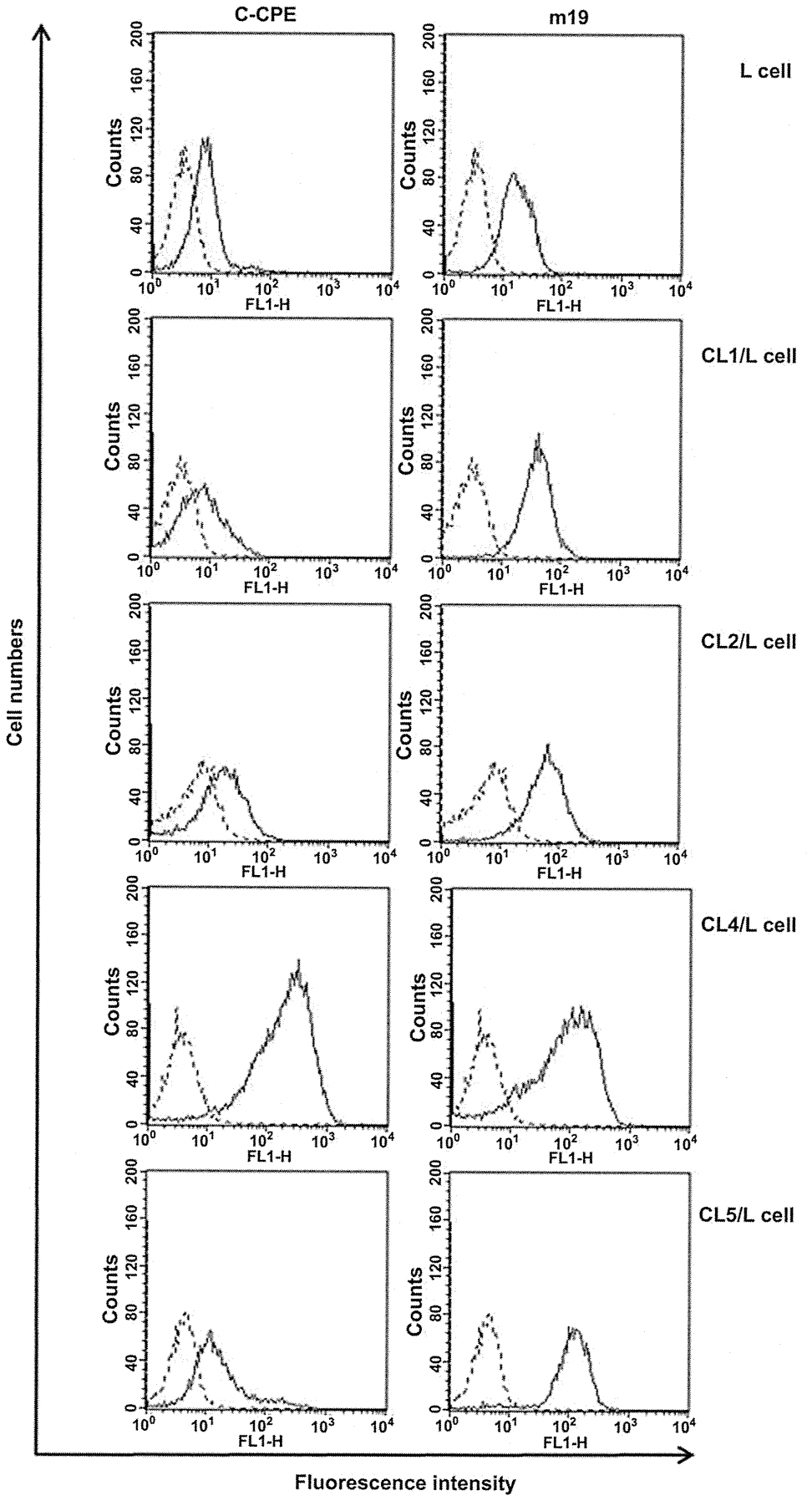

Fig. 4. FACS analysis of the interaction between m19 and CLs-cells. CLs-L cells were treated with C-CPE or m19. The bound C-CPE or m19 was detected by labeled secondary antibodies. Lined histograms indicate the level of reactivity of C-CPE or m19; dotted lined histograms indicate background binding level of anti-his tag and FITC-labeled antibodies without C-CPE or m19. The binding cells were detected by FACS analysis as described in the Materials and Methods.

a triple substituted C-CPE mutant with the same three common mutations: the triple mutant bound to CL1-BV but not to wild-BV (Fig. 3A). We prepared a series of single or double-substituted mutants (Table 3). All of the single and double mutants bound to CL1-BV (Fig. 3B). The double substituted mutant at 307 and 313 had the highest affinity to CL1-BV among the mutants (Fig. 3B). These findings indicate that Arg and His at positions 307 and 313, respectively, might be critical for the interaction of the C-CPE mutants with CL1. The isoelectric point (pI) values of Ser, Arg and His were 5.68, 10.76 and 7.59, respectively. We prepared a series of double substituted C-CPE mutants, changing Ser resides to His (pI, 7.59), Lys (pI, 9.8) or Arg (pI, 10.76), to investigate the effect of charge at positions 307 and 313 on CL1-binding. Increase and decrease in the charge at position 307 and 313, respectively, strengthened the interaction with CL1 (Fig. 3C). We also prepared double Ala- or Asp-substituted C-CPE mutants at position 307 and 313 (Ala, pI: 6.0; Asp, pI: 2.77); decrease in the charge attenuated binding to CL1 (Fig. 3D). These findings are consistent with the structural analysis of m19. Therefore, an electrostatic interaction may be involved in the binding of C-CPE mutants to CL1.

m19 interacts with CL1 via electrostatic forces, thus other CL members with a negatively charged C-CPE binding region may interact with m19. A series of chimeric analyses revealed that the region of CLs from the Asn at position 149 to the Met at position 160 may determine sensitivity of CPE (CPE sensitivity-related region; CPE-SR) [47]. The pI values of CPE-SRs are 9.70, 4.18, 4.18 and 4.18 in CL4, CL1 CL2 and CL5, respectively. A FACS analysis in CLs-expressing cells confirmed the CL member specificity for m19. C-CPE bound to CL4 but not CL1, CL2 and CL5. In contrast, m19 bound to CL1, CL2, CL4 or CL5-expressing cells (Fig. 4). Therefore, m19 may be a more broadly specific CL binder.

3.4. Effects of m19 on epithelial barriers

Caco-2 monolayer cell sheets are a common model for the evaluation of TJ barriers [48]. We compared the TJ-barrier–modulating activity of m19 and C-CPE in Caco-2 monolayer cell sheets. Treatment of the cells with C-CPE or m19 resulted in decreased TEER values (Fig. 5A); after removal of C-CPEs, the TEER values increased (Fig. 5B). The TJ-barrier-modulating activity of 20 μg/ml m19 was comparable to that of 50 μg/ml C-CPE, which indicates that m19 had stronger TJ-barrier-modulating activity than C-CPE.

There are two intercellular contacts in epithelial monolayer cell sheets: the bicellular junction between two adjacent cells and the tricellular junction on the corners at which three adjacent cells are joined [49,50]. The epithelial barrier is composed of bicellular junctions and tricellular junctions. Tricellulin is a key and functional component of tricellular junctions [51]. Tricellulin interacts with CLs in the plasma membrane [52]. We investigated the influence of m19 on epithelial barrier function in an epithelial barrier model using bicellularly tricellulin-expressing MDCK II cells developed by Krug et al. [35]. Treatment of MDCK II cells over-expressing tricellulin (TRa-8) or vector controls (V1) with 20 μg/ml C-CPE or m19 decreased the TEER values (Fig. 6A). A detailed characterization of TEER by two-path impedance spectroscopy revealed that the decrease was associated with a strong decrease of the paracellular resistance (R^{para}), while the transcellular resistance (R^{trans}) remained unchanged in both V1 cells and Tra-8 cells (Fig. 6B and C). This led to a decrease in the epithelial resistance (R^{epi}), which is TEER after subtraction of the subcellular resistance given by the filter supports (Fig. 6B and C). These findings indicate that m19 enhanced the paracellular permeability. Additional macromolecular fluxes supported the fact that C-CPE and m19 interact with CLs but not with tricellulin, as the permeability for FD-4 remained unchanged after C-CPE or m19 incubation (Fig. 6D).

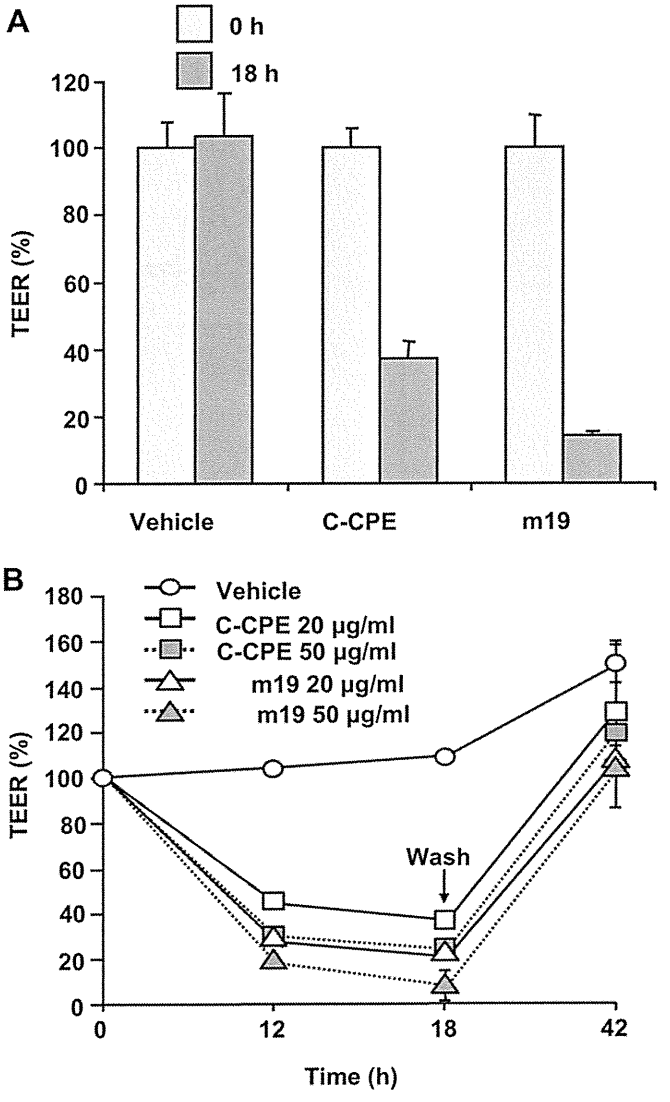

Fig. 5. Effect of m19 on TJ-integrity in Caco-2 monolayer cell sheets. A, B) Trans-epithelial electrical resistance (TEER) measurement. Caco-2 cells were seeded in BD BioCoat™ Fibrillar Collagen Cell Culture Inserts (BD Biosciences, Franklin Lakes, NJ) at a subconfluent density. The TEER of the Caco-2 monolayer cell sheets on the chamber was monitored with a Millicell-ERS epithelial volt-ohmmeter (Millipore, Billerica, MA). The Caco-2 monolayers were cultured for 5 days, and then treated with C-CPE or m19 on the basal side of the insert. The cells were exposed to the C-CPEs for 18 h (A), washed with medium to remove C-CPEs, and then cultured for an additional 24 h. Changes in TEER values were monitored during the C-CPE treatment (B). Relative TEER values were calculated as the ratio of TEER values at 0 h. The TEER values were normalized by the area of the Caco-2 monolayer, and the TEER value of a blank Transwell™ chamber (background) was subtracted. Data are presented as means ± SD ($n = 3$).

Thus, the observed effects were not mediated by tricellulin. C-CPE and m19 had similar TJ-barrier modulating activities. The discrepancy between Caco-2 cells and the MDCK cells will be addressed in the Discussion section.

We investigated effects of m19 on the localization of TJ-components by using anti-occludin, anti-tricellulin, and anti-CL1, 2, 3, 4, and 7 antibodies in an immunofluorescent analysis: there were no observable changes in the localization of each of the analyzed TJ proteins in the C-CPE or m19-treated cells (Fig. 7A–D, Suppl. Fig. 2A–H), indicating that disruption of the paracellular barrier may be due to inhibition of the adjacent intercellular interaction of CL strands caused by their interaction with the extracellular domains of CL.

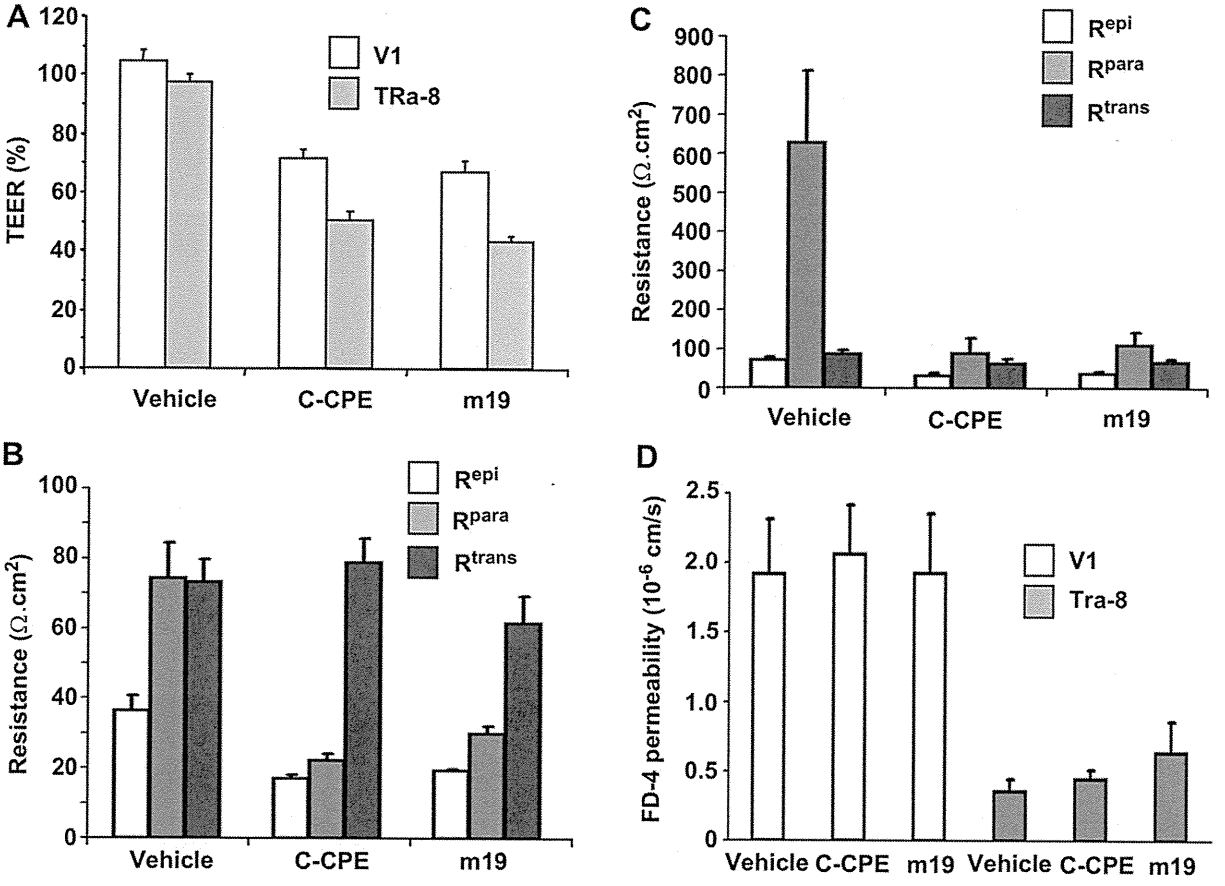

Fig. 6. Effects of m19 on the epithelial barrier in tricellulin-overexpressing MDCK II cells. A) TEER assay. Mock-expressing MDCK II cells (V1) or tricellulin-expressing MDCK II cells (TRa-8) were treated with C-CPE or m19 at 20 μg/ml for 3 h. The TEER was measured at 2 and 3 h. The TEER changes between 2 and 3 h were calculated as the ratio of TEER value at 2 h. The TEER was measured as described in Materials and Methods. Data are presented as means ± SE (n = 12–17). B, C) Effects of m19 on the paracellular resistance. V1 cells (B) or TRa-8 cells (C) were subjected to two-path impedance spectroscopy analysis as described in Materials and Methods. Data are presented as means ± SE (n = 5 or 6). D) Permeability for FD-4. V1 cells or TRa-8 cells were treated with C-CPE or m19 at 20 μg/ml for 3 h and flux for FD-4 was determined as described in Materials and Methods. Data are presented as means ± SE (n = 6 or 7).

3.5. Mucosal absorption-enhancing effects of m19

Finally, we investigated the effect of m19 on jejunal absorption by using an *in situ* loop assay and dextran with a molecular mass of 4000 Da (FD-4) as a model drug. C-CPE treatment increased plasma FD-4 levels in a time-dependent manner, reaching a maximal concentration of 3.0 μg/ml; in contrast, m19 enhanced jejunal absorption of FD-4 more than C-CPE, reaching a maximal concentration of 5.3 μg/ml (Fig. 8A). The AUC value of the m19-treated group was 2.1-fold that of the C-CPE-treated group (Fig. 8B). These results suggest that m19 is a more potent mucosal absorption enhancer than C-CPE.

4. Discussion

CL is a promising target for pharmaceutical therapy. However, CL has low antigenicity, and most attempts to prepare a monoclonal antibody against the extracellular loop region of CL have been unsuccessful. The three-dimensional structure of CL has never been determined, so it is impossible to perform a theoretical design of a CL binder based on structural information. We developed a screening system for CL binders by using a BV system and a C-CPE phage display library [30]. We successfully identified C-CPE mutants that bind to CL1, CL2, CL4 and CL5 by using this screening system. We determined the functional domain, and evaluated effects of the CL binder on modulation of the TJ-barrier to enhance mucosal absorption.

Previous reports indicate that CPE shows almost no interaction with CL1 [21,47,53]. We identified three CL1-binding C-CPE mutants, m19, m36 and m86, in which there were three common substitutions of Ser residues for Pro, Arg and His at positions 305, 307 and 313, respectively. In particular, double substitutions of Ser with Arg and His at positions 307 and 313, respectively, are important for interaction with CL1. Kimura et al. found that the CPE-binding region of CL3/4 (CPE-sensitive region; CPE-SR) may be positively charged and the CL3/4-binding region of CPE may be negatively charged; they proposed an electrostatic interaction model [47]. The pI value of CPE-SR in CL1, CL3 and CL4 is 4.18, 6.53 and 9.70, respectively [47]. Therefore, one possible explanation for binding of the C-CPE mutants to CL1 may be the increase of positively charged residues in the CL-binding region. C-CPE has 9 β-sheets and 1 α-helix, and the loop domain between β8- and β9-sheets may be the CL-binding domain [46]. Ser residues at positions 307 and 313 are located in the loop domain and the β9 sheet, respectively; changing Ser residues to Arg and His, respectively, may form a more positively charged CL-binding domain than C-CPE, leading to increased binding to CL1. Indeed, substitution of these Ser residues with Ala (pI, 6.0) or Asp (pI, 2.77) did not allow binding to CL1. These findings suggest that electrostatic interactions between C-CPE mutants and CL1 may be partially involved in their binding. In fact, the pI value of CPE-SR in CL5 was similar (4.18) to that of CL1, and also bound to

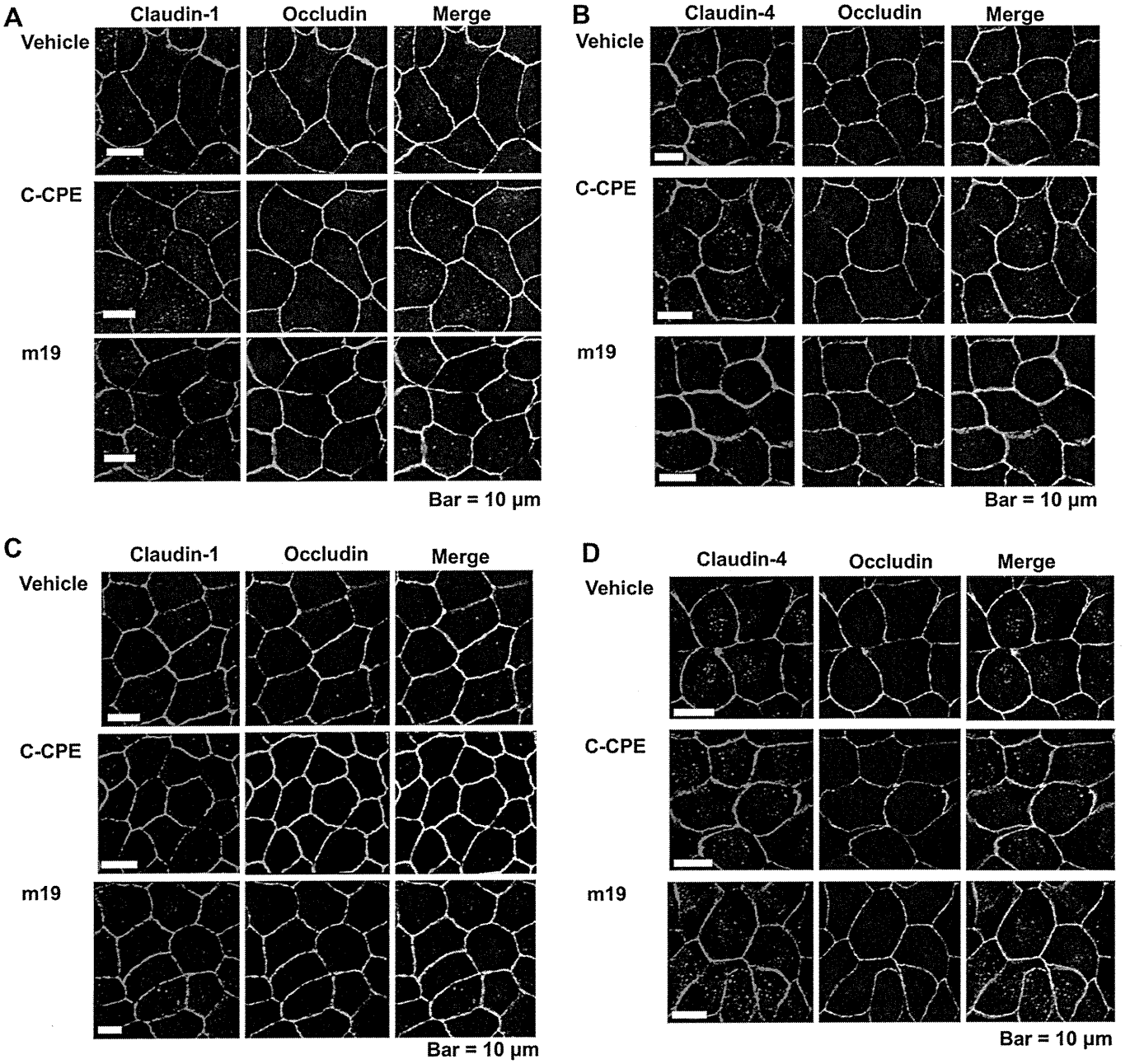

Fig. 7. Effects of m19 on localization of TJ-components. V1 cells (A, B) or TRa-8 cells (C, D) were treated with C-CPE or m19 at 20 μg/ml for 4 h. The cells were fixed with methanol and analyzed by immunofluorescence as described in Materials and Methods. CL1 (A and C), CL4 (B and D). CLs are stained red, and occludin green. Occludin was used as a TJ-marker.

m19. CL4 may interact with C-CPE at Tyr residues at positions 306, 310 and 312 and Leu at position 315. These residues form a negatively charged cleft [47]. Substitution of Ser with Arg at position 307 and Ser with His at position 313 may be important for the interaction of m19 with CL1. The binding motif for CL1 and CL4 may be different in m19. The cleft for CL4 might have a wide surface. In contrast, the motif for CL1 might be much smaller than that of CL4. An ELISA assay showed that m19 interacted much more weakly with CL1 than with CL4 (data not shown). These amino acid changes could also affect the secondary structure of the binding, which could then alter the binding affinity. Further kinetic and structural analyses of the interaction between m19 and CLs are needed.

Compared to C-CPE, m19 showed higher TJ-modulating activity in Caco-2 monolayer cell sheets and jejunal absorption-enhancing activity in rat; however, m19 showed similar TJ-modulating activity in MDCK II cells. Expression of CL4, 11 or 15 increases TJ-integrity in MDCK II cells. In contrast, expression of CL4 increases TJ-integrity in LLC-PK1 cells, but expression of CL11 or 15 decreases it [54]. CL5 is ubiquitously expressed in endothelial cells and is critical for the blood-brain-barrier [12,55]. Therefore, the difference in the activity of m19 may be due to differences in the properties of the TJ-seals in each of the assay systems: Caco-2 cells are human colon cells, MDCK II cells are canine kidney cells and rat jejunum is used in mucosal absorption of dextran.

Tricellulin has been shown to interact with CLs in the plasma membrane [52], but eventual changes in interaction due to binding of C-CPEs to CLs had no effect on macromolecular permeability regulated by tricellulin. Tricellulin also was excluded as interaction

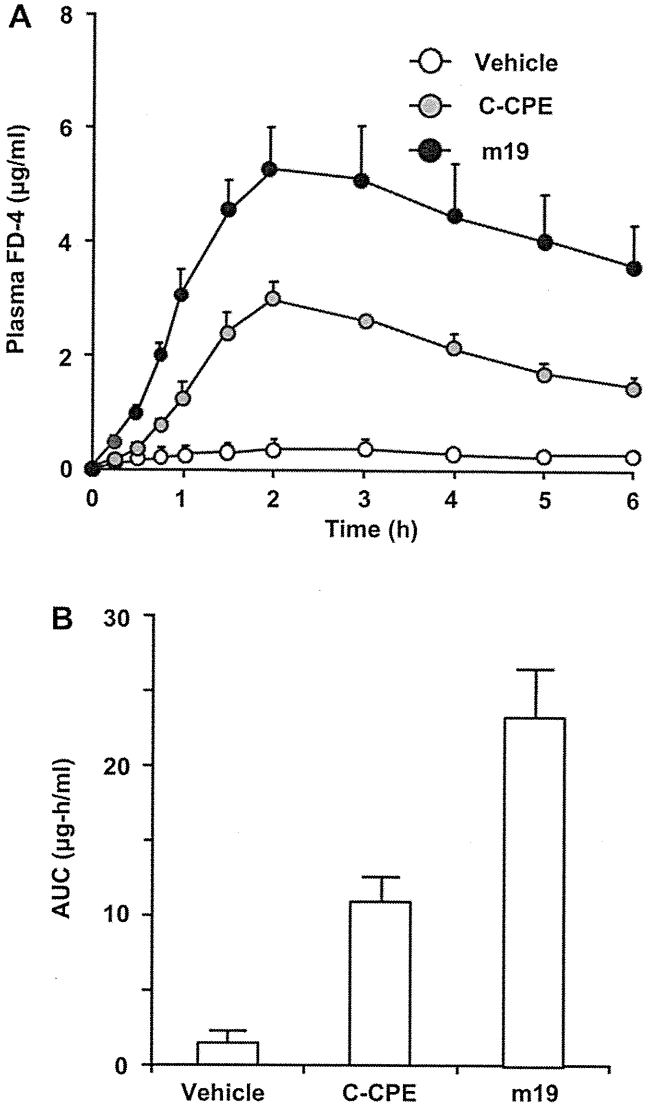

Fig. 8. Mucosal absorption of FD-4 by m19. Jejunum were treated with 2.0 mg/ml FD-4 and C-CPEs. Time-course changes in plasma FD-4 levels (A) and AUC from 0 to 6 h (B) were analyzed as described in Materials and Methods. Data are presented as means ± SE (n = 4–9).

partner for C-CPE and m19. Therefore effects that were not reflected by the cell culture model are responsible for the increase of macromolecular permeability in the jejunum which is not determined by CLs.

Preparation of CL is a requisite for screening CL binders. However, CL4 is the only CL with an established preparation method [56]. We attempted to screen the C-CPE mutant library by using CL1-expressing cells, but we did not successfully identify CL1 binders. Functional membrane proteins such as cell-surface proteins are heterologously expressed in their native forms on BVs [33,34,57]. Interactions between membrane proteins can be detected by using receptor-displaying and ligand-displaying BV [34]. CL-BV can work as a screen for CL binders by using CL4-BV and a CL4 binder, C-CPE [30]. The present study successfully identified CL1 binders from the library by using CL1-BV. We anticipate that CL-BV will be useful for the preparation of peptides and antibodies that act as CL binders.

Several groups have successfully prepared CL binders. Offner et al. prepared polyclonal antibodies against the extracellular domains of CL3 and CL4 [58], Ling et al. screened CL4 binding peptides by using a 12-mer peptide phage display library and CL4-expressing cells [59], and and Romani et al. screened scFv against CL3 by using a human antibody phage display library [60]. Suzuki et al. developed monoclonal antibodies to CL4 and CL3/4 by using mice with autoimmune disease [61,62]. Fofana et al. established a monoclonal antibody to CL1, which prevented infection by Hepatitis C virus in hepatocytes [63]. However, the TJ-modulating activities of these CL binders have never been reported; thus, C-CPE and its mutants, including m19, were the only known CL modulators [20]. The findings of the present study indicate that a BV screening system with a C-CPE library may be a powerful method to develop CL modulators.

5. Conclusions

We report here the preparation of broadly specific CL binders to CL1, CL2, CL4 and CL5. The electrostatic charge in the loop region between the β8 and β9 sheets may be critical for the interaction between the C-CPE mutants and CLs. The optimal modulation of the electrostatic charge of the CL binding region of C-CPE is an important part of the strategy for development of CL binders, contributing to CL-targeted drug development.

Acknowledgements

We thank Drs. S. Tsunoda (National Institute of Biomedical Innovation, Japan) and Y. Tsutsumi (Osaka University, Japan) for their kind instructions on the use of phage display technology. We also thank Drs. Y. Horiguchi (Osaka University, Japan), S. Tsukita (Kyoto University, Japan) and members of our laboratory for providing us C-CPE cDNA, CL-expressing cells and their useful comments and discussion, respectively. This work was supported by a Grant-in-Aid for Scientific Research from the Ministry of Education, Culture, Sports, Science and Technology, Japan (21689006), and by a Health and Labor Sciences Research Grant from the Ministry of Health, Labor and Welfare of Japan. A.T. and H.S. are supported by Research Fellowships from the Japan Society for the Promotion of Science for Young Scientists.

We thank beamline staff of BL44XU at SPring-8 for X-ray data collection. We also thank Academia Sinica and National Synchrotron Radiation Research Center (Taiwan) for use MX225-HE detector at BL44XU.

Appendix. Supplementary material

Supplementary material associated with this article can be found, in the online version, at doi:10.1016/j.biomaterials.2012.01.017.

References

[1] Farquhar MG, Palade GE. Junctional complexes in various epithelia. J Cell Biol 1963;17:375–412.
[2] Cassidy MM, Tidball CS. Cellular mechanism of intestinal permeability alterations produced by chelation depletion. J Cell Biol 1967;32:685–98.
[3] Wodarz A, Nathke I. Cell polarity in development and cancer. Nat Cell Biol 2007;9:1016–24.
[4] Yuki Y, Kiyono H. New generation of mucosal adjuvants for the induction of protective immunity. Rev Med Virol 2003;13:293–310.
[5] Jepson MA, Clark MA, Hirst BH. M cell targeting by lectins: a strategy for mucosal vaccination and drug delivery. Adv Drug Deliv Rev 2004;56:511–25.
[6] Ryan EJ, Daly LM, Mills KH. Immunomodulators and delivery systems for vaccination by mucosal routes. Trends Biotechnol 2001;19:293–304.
[7] Schneeberger EE, Lynch RD. The tight junction: a multifunctional complex. Am J Physiol 2004;286. C1213–C1228.
[8] Furuse M, Tsukita S. Claudins in occluding junctions of humans and flies. Trends Cell Biol 2006;16:181–8.
[9] Mineta K, Yamamoto Y, Yamazaki Y, Tanaka H, Tada Y, Saito K, et al. Predicted expansion of the claudin multigene family. FEBS Lett 2011;585:606–12.

[10] Furuse M, Sasaki H, Tsukita S. Manner of interaction of heterogeneous claudin species within and between tight junction strands. J Cell Biol 1999;147:891–903.
[11] Furuse M, Hata M, Furuse K, Yoshida Y, Haratake A, Sugitani Y, et al. Claudin-based tight junctions are crucial for the mammalian epidermal barrier: a lesson from claudin-1-deficient mice. J Cell Biol 2002;156:1099–111.
[12] Nitta T, Hata M, Gotoh S, Seo Y, Sasaki H, Hashimoto N, et al. Size-selective loosening of the blood-brain barrier in claudin-5-deficient mice. J Cell Biol 2003;161:653–60.
[13] Morin PJ. Claudin proteins in human cancer: promising new targets for diagnosis and therapy. Cancer Res 2005;65:9603–6.
[14] Rajapaksa TE, Stover-Hamer M, Fernandez X, Eckelhoefer HA, Lo DD. Claudin 4-targeted protein incorporated into PLGA nanoparticles can mediate M cell targeted delivery. J Control Release 2010;142:196–205.
[15] Tamagawa H, Takahashi I, Furuse M, Yoshitake-Kitano Y, Tsukita S, Ito T, et al. Characteristics of claudin expression in follicle-associated epithelium of Peyer's patches: preferential localization of claudin-4 at the apex of the dome region. Lab Invest 2003;83:1045–53.
[16] Evans MJ, von Hahn T, Tscherne DM, Syder AJ, Panis M, Wolk B, et al. Claudin-1 is a hepatitis C virus co-receptor required for a late step in entry. Nature 2007;446:801–5.
[17] McClane BA. *Clostridium perfringens* enterotoxin acts by producing small molecule permeability alterations in plasma membranes. Toxicology 1994;87:43–67.
[18] Katahira J, Inoue N, Horiguchi Y, Matsuda M, Sugimoto N. Molecular cloning and functional characterization of the receptor for *Clostridium perfringens* enterotoxin. J Cell Biol 1997;136:1239–47.
[19] Hanna PC, Wieckowski EU, Mietzner TA, McClane BA. Mapping of functional regions of *Clostridium perfringens* type A enterotoxin. Infect Immun 1992;60:2110–4.
[20] Sonoda N, Furuse M, Sasaki H, Yonemura S, Katahira J, Horiguchi Y, et al. *Clostridium perfringens* enterotoxin fragment removes specific claudins from tight junction strands: Evidence for direct involvement of claudins in tight junction barrier. J Cell Biol 1999;147:195–204.
[21] Fujita K, Katahira J, Horiguchi Y, Sonoda N, Furuse M, Tsukita S. *Clostridium perfringens* enterotoxin binds to the second extracellular loop of claudin-3, a tight junction integral membrane protein. FEBS Lett 2000;476:258–61.
[22] Uchida H, Kondoh M, Hanada T, Takahashi A, Hamakubo T, Yagi K. A claudin-4 modulator enhances the mucosal absorption of a biologically active peptide. Biochem Pharmacol 2010;79:1437–44.
[23] Kondoh M, Masuyama A, Takahashi A, Asano N, Mizuguchi H, Koizumi N, et al. A novel strategy for the enhancement of drug absorption using a claudin modulator. Mol Pharmacol 2005;67:749–56.
[24] Saeki R, Kondoh M, Kakutani H, Matsuhisa K, Takahashi A, Suzuki H, et al. A claudin-targeting molecule as an inhibitor of tumor metastasis. J Pharmacol Exp Ther 2010;334:576–82.
[25] Saeki R, Kondoh M, Kakutani H, Tsunoda S, Mochizuki Y, Hamakubo T, et al. A novel tumor-targeted therapy using a claudin-4-targeting molecule. Mol Pharmacol 2009;76:918–26.
[26] Ebihara C, Kondoh M, Hasuike N, Harada M, Mizuguchi H, Horiguchi Y, et al. Preparation of a claudin-targeting molecule using a C-terminal fragment of *Clostridium perfringens* enterotoxin. J Pharmacol Exp Ther 2006;316:255–60.
[27] Kakutani H, Kondoh M, Fukasaka M, Suzuki H, Hamakubo T, Yagi K. Mucosal vaccination using claudin-4-targeting. Biomaterials 2010;31:5463–71.
[28] Kominsky SL, Tyler B, Sosnowski J, Brady K, Doucet M, Nell D, et al. *Clostridium perfringens* enterotoxin as a novel-targeted therapeutic for brain metastasis. Cancer Res 2007;67:7977–82.
[29] Michl P, Buchholz M, Rolke M, Kunsch S, Lohr M, McClane B, et al. Claudin-4: a new target for pancreatic cancer treatment using *Clostridium perfringens* enterotoxin. Gastroenterology 2001;121:678–84.
[30] Kakutani H, Takahashi A, Kondoh M, Saito Y, Yamaura T, Sakihama T, et al. A novel screening system for claudin binder using baculoviral display. PLoS One 2011;6:e16611.
[31] Takahashi A, Komiya E, Kakutani H, Yoshida T, Fujii M, Horiguchi Y, et al. Domain mapping of a claudin-4 modulator, the C-terminal region of C-terminal fragment of *Clostridium perfringens* enterotoxin, by site-directed mutagenesis. Biochem Pharmacol 2008;75:1639–48.
[32] Takahashi A, Kondoh M, Masuyama A, Fujii M, Mizuguchi H, Horiguchi Y, et al. Role of C-terminal regions of the C-terminal fragment of *Clostridium perfringens* enterotoxin in its interaction with claudin-4. J Control Release 2005;108:56–62.
[33] Sakihama T, Masuda K, Sato T, Doi T, Kodama T, Hamakubo T. Functional reconstitution of G-protein-coupled receptor-mediated adenylyl cyclase activation by a baculoviral co-display system. J Biotechnol 2008;135:28–33.
[34] Sakihama T, Sato T, Iwanari H, Kitamura T, Sakaguchi S, Kodama T, et al. A simple detection method for low-affinity membrane protein interactions by baculoviral display. PLoS ONE 2008;3:e4024.
[35] Krug SM, Amasheh S, Richter JF, Milatz S, Günzel D, Westphal JK, et al. Tricellulin forms a barrier to macromolecules in tricellular tight junctions without affecting ion permeability. Mol Biol Cell 2009;20:3713–24.
[36] Battye TG, Kontogiannis L, Johnson O, Powell HR, Leslie AG. iMOSFLM: a new graphical interface for diffraction-image processing with MOSFLM. Acta Crystallogr D Biol Crystallogr 2011;67:271–81.
[37] Evans P. Scaling and assessment of data quality. Acta Crystallogr D Biol Crystallogr 2006;62:72–82.
[38] Winn MD, Ballard CC, Cowtan KD, Dodson EJ, Emsley P, Evans PR, et al. Overview of the CCP4 suite and current developments. Acta Crystallogr D Biol Crystallogr 2011;67:235–42.
[39] Long F, Vagin AA, Young P, Murshudov GN. BALBES: a molecular-replacement pipeline. Acta Crystallogr D Biol Crystallogr 2008;64:125–32.
[40] Emsley P, Cowtan K. Coot: model-building tools for molecular graphics. Acta Crystallogr D Biol Crystallogr 2004;60:2126–32.
[41] Murshudov GN, Vagin AA, Dodson EJ. Refinement of macromolecular structures by the maximum-likelihood method. Acta Crystallogr D Biol Crystallogr 1997;53:240–55.
[42] Krug SM, Fromm M, Gunzel D. Two-path impedance spectroscopy for measuring paracellular and transcellular epithelial resistance. Biophys J 2009;97:2202–11.
[43] Amasheh M, Grotjohann I, Amasheh S, Fromm A, Soderholm JD, Zeitz M, et al. Regulation of mucosal structure and barrier function in rat colon exposed to tumor necrosis factor alpha and interferon gamma in vitro: a novel model for studying the pathomechanisms of inflammatory bowel disease cytokines. Scand J Gastroenterol 2009;44:1226–35.
[44] Kirschner N, Houdek P, Fromm M, Moll I, Brandner JM. Tight junctions form a barrier in human epidermis. Eur J Cell Biol 2010;89:839–42.
[45] Kominsky SL. Claudins: emerging targets for cancer therapy. Expert Rev Mol Med 2006;8:1–11.
[46] Van Itallie CM, Betts L, Smedley 3rd JG, McClane BA, Anderson JM. Structure of the claudin-binding domain of *Clostridium perfringens* enterotoxin. J Biol Chem 2008;283:268–74.
[47] Kimura J, Abe H, Kamitani S, Toshima H, Fukui A, Miyake M, et al. *Clostridium perfringens* enterotoxin interacts with claudins via electrostatic attraction. J Biol Chem 2010;285:401–8.
[48] Meunier V, Bourrie M, Berger Y, Fabre G. The human intestinal epithelial cell line Caco-2; pharmacological and pharmacokinetic applications. Cell Biol Toxicol 1995;11:187–94.
[49] Staehelin LA. Further observations on the fine structure of freeze-cleaved tight junctions. J Cell Sci 1973;13:763–86.
[50] Staehelin LA, Mukherjee TM, Williams AW. Freeze-etch appearance of the tight junctions in the epithelium of small and large intestine of mice. Protoplasma 1969;67:165–84.
[51] Ikenouchi J, Furuse M, Furuse K, Sasaki H, Tsukita S, Tsukita S. Tricellulin constitutes a novel barrier at tricellular contacts of epithelial cells. J Cell Biol 2005;171:939–45.
[52] Ikenouchi J, Sasaki H, Tsukita S, Furuse M, Tsukita S. Loss of occludin affects tricellular localization of tricellulin. Mol Biol Cell 2008;19:4687–93.
[53] Winkler L, Gehring C, Wenzel A, Müller SL, Piehl C, Krause G, et al. Molecular determinants of the interaction between *Clostridium perfringens* enterotoxin fragments and claudin-3. J Biol Chem 2009;284:18863–72.
[54] Van Itallie CM, Fanning AS, Anderson JM. Reversal of charge selectivity in cation or anion-selective epithelial lines by expression of different claudins. Am J Physiol 2003;285:F1078–84.
[55] Morita K, Furuse M, Fujimoto K, Tsukita S. Claudin multigene family encoding four-transmembrane domain protein components of tight junction strands. Proc Natl Acad Sci U S A 1999;96:511–6.
[56] Mitic LL, Unger VM, Anderson JM. Expression, solubilization, and biochemical characterization of the tight junction transmembrane protein claudin-4. Protein Sci 2003;12:218–27.
[57] Loisel TP, Ansanay H, St-Onge S, Gay B, Boulanger P, Strosberg AD, et al. Recovery of homogeneous and functional beta 2-adrenergic receptors from extracellular baculovirus particles. Nat Biotechnol 1997;15:1300–4.
[58] Offner S, Hekele A, Teichmann U, Weinberger S, Gross S, Kufer P, et al. Epithelial tight junction proteins as potential antibody targets for pan-carcinoma therapy. Cancer Immunol Immunother 2005;54:431–45.
[59] Ling J, Liao H, Clark R, Wong MS, Lo DD. Structural constraints for the binding of short peptides to claudin-4 revealed by surface plasmon resonance. J Biol Chem 2008;283:30585–95.
[60] Romani C, Comper F, Bandiera E, Ravaggi A, Bignotti E, Tassi RA, et al. Development and characterization of a human single-chain antibody fragment against claudin-3: a novel therapeutic target in ovarian and uterine carcinomas. Am J Obstet Gynecol 2009;201(70):e1–9.
[61] Kato-Nakano M, Suzuki M, Kawamoto S, Furuya A, Ohta S, Nakamura K, et al. Characterization and evaluation of the antitumour activity of a dual-targeting monoclonal antibody against claudin-3 and claudin-4. Anticancer Res 2010;30:4555–62.
[62] Suzuki M, Kato-Nakano M, Kawamoto S, Furuya A, Abe Y, Misaka H, et al. Therapeutic antitumor efficacy of monoclonal antibody against Claudin-4 for pancreatic and ovarian cancers. Cancer Sci 2009;100:1623–30.
[63] Fofana I, Krieger SE, Grunert F, Glauben S, Xiao F, Fafi-Kremer S, et al. Monoclonal anti-claudin 1 antibodies prevent hepatitis C virus infection of primary human hepatocytes. Gastroenterology 2010;139:953–64.

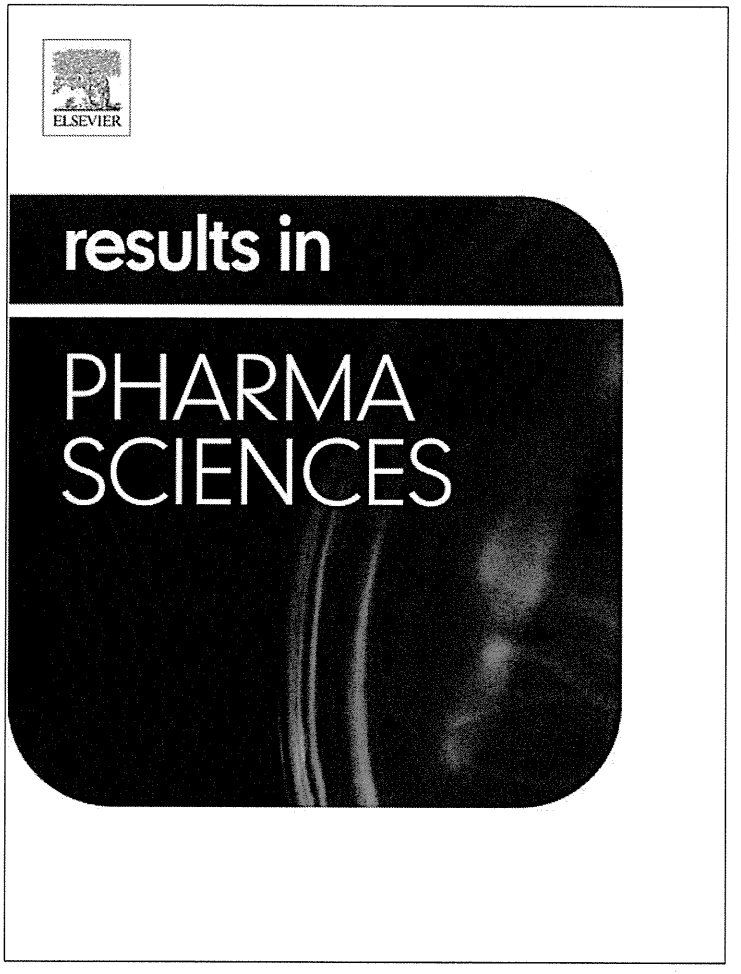

(This is a sample cover image for this issue. The actual cover is not yet available at this time.)

Results in Pharma Sciences 2 (2012) 16–22

Contents lists available at SciVerse ScienceDirect

Results in Pharma Sciences

journal homepage: www.elsevier.com/locate/rinphs

Oil-in-water emulsion lotion providing controlled release using 2-methacryloyloxyethyl phosphorylcholine n-butyl methacrylate copolymer as emulsifier

Akiko Ishikawa, Makiko Fujii*, Kumi Morimoto, Tomomi Yamada, Naoya Koizumi, Masuo Kondoh, Yoshiteru Watanabe

Showa Pharmaceutical University, 3-3165, Higashi-Tamagawagakuen, Machida, Tokyo 194-8543, Japan

ARTICLE INFO

Article history:
Received 9 December 2011
Received in revised form
18 January 2012
Accepted 24 January 2012
Available online 1 February 2012

Keywords:
Skin penetration
Nanocapsule
Sustained release
Diphenhydramine
Topical application

ABSTRACT

Lotion is a useful vehicle for active ingredients used to treat skin disease because it can be applied to the scalp, can cover large areas of skin, and it is easy to spread due to low viscosity. An emulsion lotion (EL) containing 2-methacryloyloxyethyl phosphorylcholine n-butyl methacrylate copolymer (PMB) as an emulsifier that provides controlled-release was developed. Diphenhydramine (DPH) was used as a model drug. Formulation with 5% DPH, 5% soybean oil, and 4% PMB in water was emulsified using a high-pressure homogenizer. Polysorbate 80 (TO) was used instead of PMB for comparison. They were applied *in vitro* to Yucatan micropig intact or stripped skin at a practical dose (2 $\mu L/cm^2$). For stripped skin, penetration of DPH from 4% PMB EL was slower than that from 1% TO EL; results for intact skin were similar. The same phenomenon was observed with application to rabbit skin *in vivo*. When 4% PMB EL dried on the skin, it made a thin film matrix incorporating the oil phase, which controlled the release of DPH. The release rate could be controlled by the ratio of oil phase to PMB. The EL with PMB shows promise as a vehicle for long-acting treatment of skin diseases.

1. Introduction

Skin is an attractive site for systemic drug delivery, and many new vehicles have been developed that promote good skin permeation [1]. In addition, topical delivery of drugs for skin diseases is effective with few systemic side effects. The choice of vehicle is made based on the type of skin condition. Ointments, creams, and lotions are common dosage forms. Lotion is especially convenient for use on the scalp (or other site with hair) or to cover large areas because it has low viscosity and is easy to spread. However, lotion does possess some disadvantages: drugs with low water solubility require solubilizing agents and procedures; the formulation of lotion is affected by the vaporization of some ingredients after application to skin that leaves drug and additives on the skin surface, which can cause irritation; and the amount of drug per unit area is relatively small and the duration of effectiveness is short when applied on damaged skin because lotion does not provide controlled release as an ointment does [10]. Thus, a new vehicle consisting of an oil-in-water (o/w) emulsion lotion (EL), which can accommodate poorly water-soluble drugs in the oil phase and provides controlled release, was developed.

Polymers are often employed to control drug release, with carboxyvinyl polymer and hydroxypropylmethyl cellulose commonly used for this purpose. However, these polymers do not have solubilizing or emulsifying properties. Therefore, a polymer is needed with solubilizing or emulsifying properties that can provide controlled release. The PMB, 2-methacryloyloxyethyl phosphorylcholine (MPC) n-butyl methacrylate (BMA) copolymer, possesses both hydrophilic and hydrophobic characteristics. The MPC also has excellent biocompatibility [12] and is used for contact lens [3]. Since the MPC unit is extremely hydrophilic, the copolymer with the MPC unit can be dissolved in water. Some drugs can be solubilized by PMB [4,8,5]. The PMB also is used in cosmetics to moisturize skin [6]. Since the molecular weight of PMB is as high as 600,000, it may remain on the skin surface and so is likely to be safer than conventional surfactant which sometimes irritates skin. We previously reported that skin penetration of 2-ethylhexyl methoxycinnnamate, which is a UV absorber, was inhibited when PMB was used as an emulsifier [2]. Thus, PMB was tested as an emulsifier for the EL that provides sustained drug release. Diphenhydramine (DPH), which is a widely used antihistamine for allergy relief, is a liquid insoluble in water, and capable of rapidly penetrating skin [9], was used as the model

* Corresponding author. Tel.: +81 42 721 1556; fax: +81 42 723 3585.
E-mail address: fujii@ac.shoyaku.ac.jp (M. Fujii).

2211-2863/$ - see front matter © 2012 Elsevier B.V. All rights reserved.
doi:10.1016/j.rinphs.2012.01.001

drug in this study. EL containing DPH and PMB was prepared, and penetration of DPH into skin was determined through *in vitro* and *in vivo* experiments. In addition, the mechanism of sustained release of DPH from EL was studied.

2. Materials and methods

2.1. Materials

DPH (JP grade) was obtained from Nippon Bulk Yakuhin (Osaka). PMB (Lipidure-PMB®; MPC: BMA=8:2) was supplied by NOF Co., Ltd (Tokyo) as a 5% solution. Polyoxyethylene (20) sorbitan monooleate (TO) was a gift from Nikko Chemicals Co., Ltd (Tokyo). Soybean oil (SO, reagent grade) was purchased from Wako Pure Chemical Industries (Osaka). Other reagents were of analytical grade.

2.2. Preparation of lotion

DPH itself or DPH mixed with SO was used as oil phase, and a PMB solution of the appropriate concentration was added to the oil phase. Pre-emulsification was performed using a mixer (Quick Homomixer LR-1 Mizuho, Osaka) at 3000 rpm for 2 min. The mixture was then introduced into a high-pressure homogenizer (Microfluidizer®, Mizuho) and passed through 10 times at a pressure of 10,000 psi. The standard formulation consisted of 5% DPH, 5% SO, 4% PMB, and water (PMB4% EL). For preparation of PMB8% EL, a commercial PMB solution was lyophilized and the PMB powder was dissolved in water at an appropriate concentration. TO was used as emulsifier instead of PMB for comparison.

An EL consisting of 10% DPH, 10% SO, and 2% TO was prepared using the procedure described above, followed by mixing at the same volume of 8% PMB solution (TO1%+PMB4% EL). The standard formulation prepared pre-emulsification was used as comparison (PMB4%-pre EL).

The mean diameter of droplets in the prepared EL was measured by dynamic light scattering (DLS, ELS-800, Otsuka Electric, Osaka) at a dilution of 200. The mean diameter was calculated using cumulant method. Each sample was measured doublicated and at least 3 samples were used.

Particle shape was observed with transmission electron microscopy (TEM) (JEM1200EX, Jeol, Tokyo) at 80 kV with negative staining by phosphotungstic acid. It was done in Hanaichi Ultra-Structure Research Institute (Okazaki, Japan).

2.3. In vitro skin permeation study

The skin permeation study was performed under two conditions, infinite dose conditions (infinite dose) and the practical small amount application recommended in OECD guideline 428 (practical dose).

Yucatan micropig (YMP) skin sets frozen at −80 °C were purchased from Charles River Japan, Inc. (Kanagawa, Japan). Skin was thawed at 20–25 °C for approximately 30 min, followed by removal of the adhering fat layer using scissors and a grater, and cut into appropriate sizes (intact skin). YMP intact skin has the stratum corneum (SC) consists of about 20-layer, a part of SC was removed from intact skin with adhesive tape (Scotch®313, 3 M, Tokyo) 15 times (stripped skin) to make a model of damaged skin. Skin penetration was measured in a modified Franz diffusion cell apparatus [effective area, 1.1 cm^2; receptor, 16 mL isotonic phosphate buffered solution (pH 7.1) maintained at 37 °C mixed with a star-head magnet at 600 rpm].

For the infinite dose condition, skin was mounted directly on the cell, a 2.0-mL aliquot of EL was poured into the donor phase, and the donor phase was occluded. At predetermined times, 200-μL aliquots were withdrawn from the receptor compartment. The same volume of fresh solution was added to the receptor compartment after withdrawal to maintain constant volume. At 27 h after application, skin was removed from the cell, washed with purified water, gently dried, and used for further testing.

For the practical dose, EL was spread on the skin at 2 μL/cm^2, and the skin was mounted on the cell. The donor phase was not occluded. At 4, 14, and 24 h after application, 200-μL aliquots were withdrawn from the receptor compartment and skin was removed from the cell and used for further tests without washing to determine the mass balance of DPH.

After the skin permeation study, skin was stripped 10 times (intact skin) or 5 times (stripped skin) with adhesive tape (Scotch CC1820-Bx-J, 3 M) to determine the amount of DPH near the surface of skin, followed by soaking in methanol. The skin was then separated into the epidermis and dermis by the heat separation method [7]. Methanol was added to each part, and the epidermis and dermis were homogenized and centrifuged at 3000 rpm for 5 min, and the supernatant filtered with a membrane filter (0.45 μm for epidermis and 0.20 μm for dermis). The DPH concentration in the solutions obtained was determined using HPLC.

2.4. In vivo skin permeation study

Rabbits (Japanese white, males, body weight *ca.* 3 kg) were used for the *in vivo* skin permeation study. The hair of the back was removed using an electric hair clipper followed by depilatory cream the day before application. The EL was spread at 2 μL/cm^2. After 4-h application, SC was stripped 5 times with adhesive tape, followed by sacrifice of the rabbit and isolation of the skin. The skin was separated into the epidermis and dermis using the heat separation method. The remaining process followed was the same as that of the *in vitro* study. This study was approved by the Ethics Committee of Showa Pharmaceutical University.

2.5. In vitro release test

Two types of release tests were arranged for the infinite and practical dose. For the infinite dose study, DPH release was determined by dialysis using a cellulose dialysis tube and JP XV dissolution test apparatus (Toyama Sangyo, Osaka). One mL of EL and 10 mL of water were placed in a rotation basket covered with a dialysis membrane filter (#36, Wako Pure Chemical). The release test was done at a rotation speed of 100 rpm, dissolution medium of 900 mL at pH 7 phosphate buffer solution. At predetermined time intervals, 5 mL of medium were removed and fresh medium was added. DPH concentration was determined by absorbance at 218 nm.

For the practical dose, release from dried EL was determined using a glass plate and oil clear paper. The EL was applied to the glass plate at 20 μL/10 cm^2 followed by drying placed in room at 25 °C for 2 h. A piece of oil clear paper (Gatsby, Mandom, Osaka) was placed on the glass plate for adsorbed oil. The amount of oil released at 0 h was calculated from the weight difference of the paper before and after oil absorption. Then, the glass plate was placed upside down on the oil clear paper for 1 or 2 h, and the test paper was changed. Amounts of DPH released at 0, 1, 2, and 4 h after drying were determined. DPH absorbed to the paper was extracted with methanol and absorbed amount was determined using HPLC.

2.6. Analytical method

DPH concentrations were determined by an HPLC instrument (Shimadzu, Kyoto) equipped with a spectrophotometric detector (SPD-6A). The DPH were eluted from the column

(Wakosil, 150 × 4.8 mm, Wako Pure Chemicals Industry, Osaka) at ambient temperature with a mobile phase of 0.1% phosphoric acid solution-methanol (55:45), at flow rate of 1 mL/min. DPH was detected at 230 nm. The retention time of DPH was about 9 min and no interference peak of skin component was observed.

2.7. Statistical analysis

The amount of DPH on or permeated into the skin was determined for at least 3 experiments and the data subjected to analysis of variance (ANOVA) followed by Dunnett's test using TO1% EL as a control. A value of $P < 0.05$ was considered significant.

3. Results and discussion

3.1. Characterization of emulsions

Various formulations of ELs were prepared and oil droplet size in ELs determined by DLS is shown in Table 1. When only DPH was used as the oil phase, oil droplet size was greater than 500 nm one day after preparation, and creaming occurred within a month, even if the PMB concentration was 4% and the Microfluidizer was used. Thus, SO (a lipophilic oil) was added to the oil phase. The DPH was mixed with SO (oil phase) then the PMB solution (water phase) was added. Pre-emulsified EL was not stable and phase separation occurred. A stable emulsion was obtained using the Microfluidizer. The size of oil droplet measured by DLS was *ca.* 200 nm for PMB ELs. PMB is a polymer, there was a possibility that PMB trap oil in its polymer chain and so called emulsion was not formed. Thus, TEM images of PMB4% EL was observed (Fig. 1). The image shows relatively uniform spheres, which size were slightly smaller than those obtained by DLS measurement (100–200 nm). It indicates that PMB is not a so called "surfactant," a stable EL was obtained with a high shear rate emulsifying.

The EL using the nonionic surfactant TO also was prepared as a control, which was stable when prepared by the same method as PMB ELs, and the droplet sizes were smaller than those of PMB ELs.

Table 1
Oil droplet size in emulsions as measured by DLS.

	Formulation (%)			Droplet size (nm)	
	DPH	SO	Emulsifier	1 Day	1 Month
PMB4% without SO	5	0	4	1473 ± 381	C
PMB1% EL	5	5	1	183 ± 8	191 ± 13
PMB4% EL	5	5	4	250 ± 29	254 ± 9
TO1% EL	5	5	1	124 ± 31	119 ± 14

C; Creaming was observed.

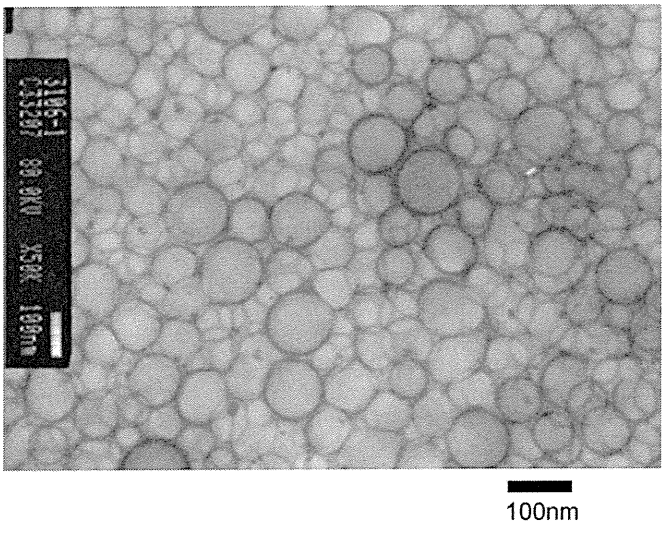

Fig. 1. TEM photograph of PMB 4% EL with negative staining by phosphotungstic acid. Bar in the photograph shows 100 nm.

3.2. Skin permeation in vitro

3.2.1. Infinite dose

The cumulative permeation of DPH from 2 mL TO1%, PMB1%, and PMB4% ELs through YMP intact skin was determined. The steady-state flux and lag time, which were calculated from the linear section of time-cumulative amount plots, and skin concentrations are shown in Table 2. No significant difference in flux or lag time was found among the formulations. Amounts of DPH in skin after application of PMB4% EL tended to be less than those of other formulations, and concentration in SC was significantly lower than that of TO1% EL.

The amount of DPH in the EL was 100 mg; the total amount of DPH that penetrated and permeated the skin was *ca.* 1 mg for all formulation. Thus, the amount of DPH was adequate and infinite conditions are maintained to 27 h after application. In contrast, the partition coefficient of DPH between SO and water (P) was high (log P=4.6), so that the amount of DPH in the water phase of the donor EL was only about 50 μg. Thus, DPH in the oil phase should be released into the water phase as the DPH in the water phase decreases due to penetration of DPH into the skin. DPH release from the oil phase appeared to be sustained for PMB4% EL. Release of DPH was determined by dialysis. Release of DPH from PMB4% EL was 25% at 1 h and 77% at 6 h, which was less than that from TO1% EL (71% at 1 h and 90% at 2 h). However, the flux of DPH through skin is not as great as release from the oil phase; thus, the difference in formulation does not affect skin permeation.

3.2.2. Practical dose

In practical use, the amount of emulsion applied onto the skin is small. Thus, the water in the EL evaporates, which changes the condition of the emulsion, disrupts its structure, can result in inversion from o/w to w/o or make a thin film consisting of non-vaporized materials, drug, oil, or surfactant. When EL was applied

Table 2
Skin permeation parameters after application of 2 mL/cm^2 of various formulations to intact skin.

	Flux (μg/cm^2/h)	Lag time (h)	SC (μg/cm^2)	Epidermis (μg/cm^2)	Dermis (μg/cm^2)	Receptor (μg)
TO1%EL	17.8 ± 3.3	5.4 ± 2.1	31.0 ± 5.9	67.7 ± 5.8	556 ± 13	381 ± 42
PMB1%EL	16.8 ± 5.5	6.4 ± 4.1	29.4 ± 10.8	70.2 ± 7.9	605 ± 54	331 ± 58
PMB4%EL	16.5 ± 1.8	7.5 ± 1.1	13.5 ± 4.3[a]	54.3 ± 2.0	489 ± 23	320 ± 18

All formulations contain 5% DPH and 5% SO.
Each value represents the mean ± S.D. of three experiments.
[a] Significantly different ($p < 0.05$) from TO1%.

on intact skin and stripped skin, the amount of DPH in SC near the surface, in the epidermis, in the dermis, and in the receptor phase was determined at 4, 14, and 24 h after application.

Fig. 2 shows the distribution of DPH in the skin and receptor phase. For intact skin (solid lines), the DPH in SC decreased with time, but about one-half of the DPH applied remained near the skin surface after 24 h application. The DPH levels in the epidermis and dermis were almost constant, *ca.* 10–20% of the dose within 24 h. The DPH in the receptor phase increased with time, but less than 20% of the applied DPH permeated within 24 h. Some points were significantly different for formulations (in SC and dermis at 4 h after application of PMB4% EL and in the receptor phase at 24 h after application), but formulation had little effect on the skin distribution of DPH. This suggests that the rate-limiting step of DPH skin permeation is related to the skin barrier, not the formulation of the EL.

For stripped skin (dashed lines), DPH in SC decreased immediately, with only 20% remaining at 4 h after application and almost none at 14 h. The DPH in the epidermis reached a peak at 4 h and then decreased at 24 h. The amount of DPH in the dermis and receptor phase tended to be high after application of TO1% and PMB1% ELs. In contrast, after application of PMB4% EL, the DPH in the SC was significantly greater, but in the dermis it was significantly less than after application of TO1% EL. In the epidermis, no significant difference among formulations was found, although the DPH level tended to be low after application of PMB4% EL.

The permeation of DPH through stripped skin was faster than that through intact skin, because the thickness of SC, main barrier of skin permeation was decreased. Ohtani et al. [10] reported that the difference in skin permeation between intact and stripped skin was greater for a lotion than for a cream or ointment. However, after application of PMB4% EL to stripped skin, the distribution of DPH was similar to that of intact skin, which suggests that the release of DPH was controlled by the vehicle for PMB4% EL.

3.3. *Skin permeation in vivo*

An *in vitro* skin permeation study showed increased skin concentration of the drug due to lack of clearance by blood flow [11].

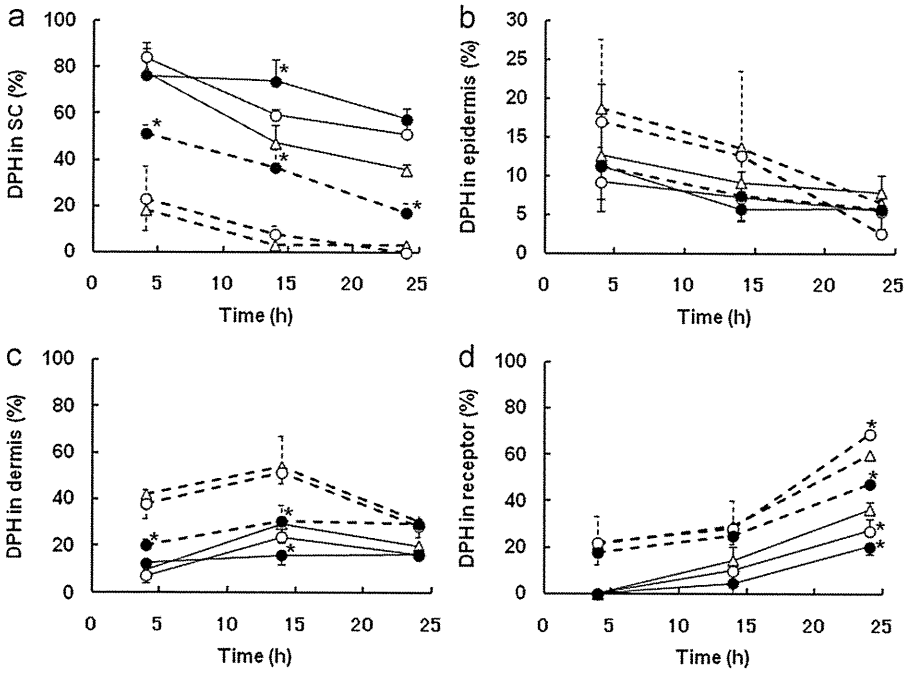

Fig. 2. Skin distribution of DPH after application of 2 μL/cm² EL to YMP skin *in vitro*. (a) Stratum corneum near the surface of skin; (b) Epidermis; (c) Dermis; (d) Receptor Solid line, intact skin; dashed line, stripped skin. △, TO1% EL; ○, PMB1% EL; ●, PMB4% EL. Each point represents the mean ± SD of three experiments. *Significantly difference *versus* TO 1% EL applied the skin with the same condition.

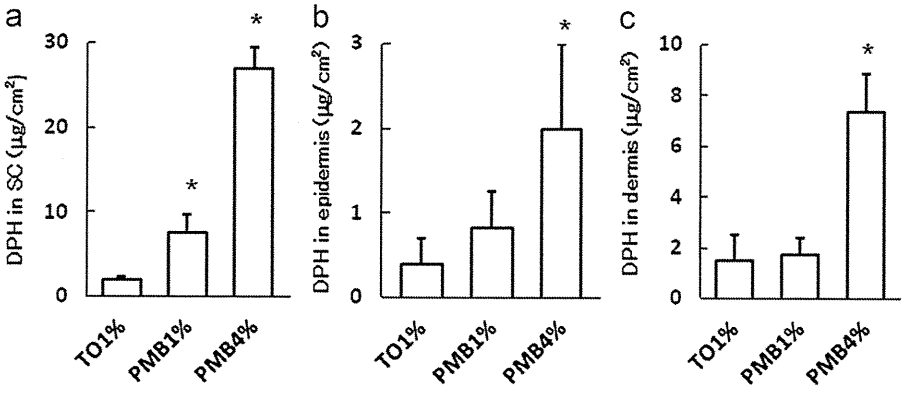

Fig. 3. Skin distribution of DPH at 4 h after application of 2 μL/cm² EL to rabbit skin *in vivo*: (a) Stratum corneum; (b) Epidermis; (c) Dermis. Each point represents the mean ± SD of three experiments. *Significantly difference *versus* TO 1% EL.